SANDIA REPORT

SAND2005-2947
Unlimited Release
Printed June 2005

Theory and Experimental Validation of SPLASH
(Single Panel Lamp and Shroud Helper)

Marvin E. Larsen and Jason M. Porter

Prepared by
Sandia National Laboratories
Albuquerque, NM 87185 and Livermore, California 94550

Sandia is a multiprogram laboratory operated by Sandia Corporation, a Lockheed Martin Company, for the United States Department of Energy under Contract DE-AC04-94AL85000.

Issued by Sandia National Laboratories, operated for the United States Department of Energy by Sandia Corporation.

Available to DOE and DOE contractors from
U.S. Department of Energy
Office of Scientific and Technical Information
P.O. Box 62
Oak Ridge, TN 37831

Telephone: (865)576-8401
Facsimile: (865)576-5728
E-Mail: reports@adonis.osti.gov
Online ordering: http://www.osti.gov/bridge

Available to the public from
U.S. Department of Commerce
National Technical Information Service
5285 Port Royal Rd
Springfield, VA 22161

Telephone: (800)553-6847
Facsimile: (703)605-6900
E-Mail: orders@ntis.fedworld.gov
Online order: http://www.ntis.gov/help/ordermethods.asp?loc=7-4-0#online

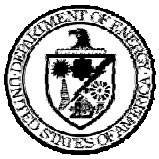

SAND2005-2947
Unlimited Release
Printed June 2005

Theory and Experimental Validation of SPLASH (Single Panel Lamp and Shroud Helper)

Marvin E. Larsen and Jason M. Porter

Sandia National Laboratories
PO BOX 5800
Albuquerque, NM 87185-0836

Abstract

The radiant heat test facility develops test sets providing well-characterized thermal environments, often representing fires. Many of the components and procedures have become standardized to such an extent that the development of a specialized design tool was appropriate. SPLASH (Single Panel Lamp and Shroud Helper) is that tool. SPLASH is implemented as a user-friendly program that allows a designer to describe a test setup in terms of parameters such as lamp number, power, position, and separation distance. Thermal radiation is the dominant mechanism of heat transfer and the SPLASH model solves a radiation enclosure problem to estimate temperature distributions in a shroud providing the boundary condition of interest. Irradiance distribution on a specified viewing plane is also estimated. This document provides the theoretical development for the underlying model. A series of tests were conducted to characterize SPLASH's ability to analyze lamp and shroud systems. The comparison suggests that SPLASH succeeds as a design tool. Simplifications made to keep the model tractable are demonstrated to result in estimates that are only approximately as uncertain as many of the properties and characteristics of the operating environment.

Acknowledgements

The authors gratefully acknowledge the interest and support of Louis Gritzo, Jim Nakos, Walt Gill, Mike Ramirez, Charles Hanks, Bennie Belone, and Jill Suo-Anttila.

Table of Contents

List of Figures

List of Tables

Nomenclature

A	area (m^2)
$\overline{B}$	Exitation vector for enclosure analysis $\varepsilon_i \sigma T_i^4$ (W/ m^2)
C_p	Specific heat (J/kg/K)
E	Emissive power, σT^4 (W/ m^2)
F , $[F]$	View factor, matrix of view factors
$[H]$	Square matrix of $h_{ij} = \delta_{ij} + (\varepsilon_i - 1)F_{ij}$
I	Irradiance (W/ m^2)
$[I]$	Identity matrix
k	Thermal conductivity (W/m/K)
P , I , D	Constants for proportional, integral, differential controller
$\overline{q}$	Vector of radiation fluxes (W/ m^2)
Q	Heat transfer rate (W)
t	Time (s)
T	Temperature (K)
TC	Thermocouple
V	Volume (m^3)
$\overline{W}$	Vector of enclosure radiosities (W/ m^2)
x , y , z	Directions in 3-space
δ_{ij}	Kronecker delta
ε	emissivity
σ	Stefan-Boltzmann constant (5.67E-8 W/K^4/ m^2)

1 Introduction

Sandia's Radiant Heat Facility makes extensive use of high power lamps to generate fire-simulating, controlled boundary conditions for thermally challenging tests. A particular panel design (Ref. [1]), accommodates up to 63 lamps. A test set utilizing the panel is shown in Figure 1. The panel can be configured with any subset of the lamp slots occupied to tailor a desired heating effect. Since all of the lamps in a panel are energized by the same electrical bus, each operates at the same power level. An inconel shroud is usually used between the lamps and the test object. In these cases the goal is to provide a uniform (or least well characterized) shroud temperature which is "seen" by the test object and understood by modelers so that analysis methods can be developed and validated. The panel is versatile and has been used at the facility in many different test configurations. In some large test configurations it is necessary to utilize multiple panels. However, many experimental arrangements are accommodated using a single panel. As many of the components and implementation practices have become standardized, it was desirable and practical to develop an easy-to-use model to approximately predict expected performance for proposed lamp and shroud geometries. SPLASH (**S**ingle **P**anel **L**amp and **S**hroud **H**elper) is the resultant model.

The SPLASH software is a Windows application with Graphical User Interfaces (GUI). SPLASH's GUI provides error checking and contemporary GUI widgets to facilitate the accurate and complete specification of component properties needed to define a lamp and panel test set up. In addition to guiding model quantitative input, SPLASH renders graphical views of the test setup and resulting predictions.

This document describes the theory used in the model and presents comparison to experiments to quantify the model's success. A separate document (Ref. [2]) is SPLASH's user manual.

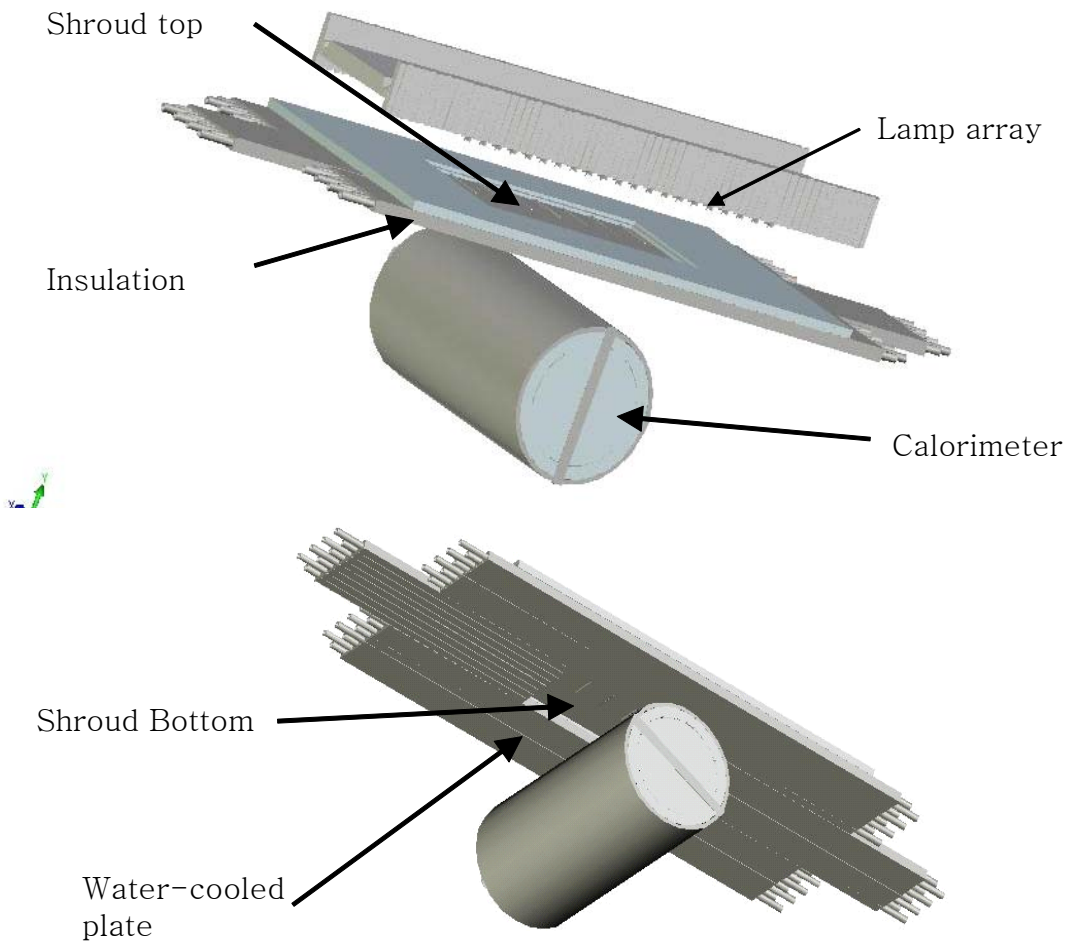

Figure 1: Schematic views of a typical single panel lamp and shroud test set.

2 SPLASH Model Description and Assumptions

2.1 Geometry and overview

Figure 2 is a schematic representation of a system including a shroud. SPLASH also has mode of operation that calculates the incident radiation on the viewing plane shown when there is no shroud present. The terms *shroud mode* and *aperture mode* will be used throughout this document to qualify discussions that pertain to only one of these modes of operation. The left part of the figure is representative of a section through the middle of the test set and perpendicular to the quartz lamps (circular lamp cross-sections are shown). In actual systems the upper cooled plate is the lamp panel ([1]). The lower cooled plate supporting insulation and the shroud may have a circular or rectangular opening defining the hot spot that irradiates the test object.

The right hand side of Figure 2 shows the geometry idealizations that are accepted to facilitate the model implementation. As shown, the lamps are replaced by flat strips in

the same plane as the bottom of the cooling plate. This simplification makes calculation of the required view factors tractable. The loss of geometric detail appears to be unimportant because, in practice, the lamp separation from the shroud is generally large compared to the geometric features in the vicinity of the lamps. In subsequent sections the success of the approach will be demonstrated.

Also shown on the right hand side of Figure 2 are symbols representing the most important physical properties of the system. $T(t)$ represents a ramp-up-and-hold temperature schedule that is a model input. In the actual hardware and the simulation in SPLASH, the power input to the lamps is a function of the difference between the temperature at the bottom center of the shroud and the specified schedule. Lamp inventory and physical dimensions of all the components are also model inputs. Model assumptions include:

1. All thermally radiating surfaces are gray, diffuse emitters and reflectors of constant emissivity.
2. Thermal radiation exchange is considered between the lamp panel and the shroud and insulation. An enclosure analysis is formulated for exchange between all the surfaces above the insulation layer (view factor calculation and energy balance considerations are discussed in Appendix A).
3. The temperatures of surfaces on the lamp panel between the lamps and that of the substrate to the insulation are specified and constant.
4. Conduction occurs through the insulation only in the direction normal to the plane layer.
5. Conduction through the shroud occurs in three directions, but the distribution of temperature through the thickness is not resolved. The temperature gradients in the lateral direction are approximated by differencing the temperatures observed in the top face. These gradients are applied through the thickness, i.e., $\frac{\partial}{\partial z}\left[\frac{\partial T}{\partial (x \text{ or } y)}\right] = 0$.
6. In shroud mode the bottom side of the shroud radiates to a uniform, specified environment temperature. The effects of radiation returned from a heating test object are not considered. In calculating flux distributions onto a viewing plane from the bottom of the shroud shadowing due to the thickness of the substrate is not considered.
7. In aperture mode a cold black surface is substituted for the shroud in performing the enclosure analysis above the shroud. The resulting radiosities from the panel and lamps are used in the calculation of incident radiation on the viewing plane. Rays from those surfaces projecting to the viewing plane must pass through the substrate aperture at its top and bottom faces (i.e., shadowing due to the thickness of the substrate is considered).

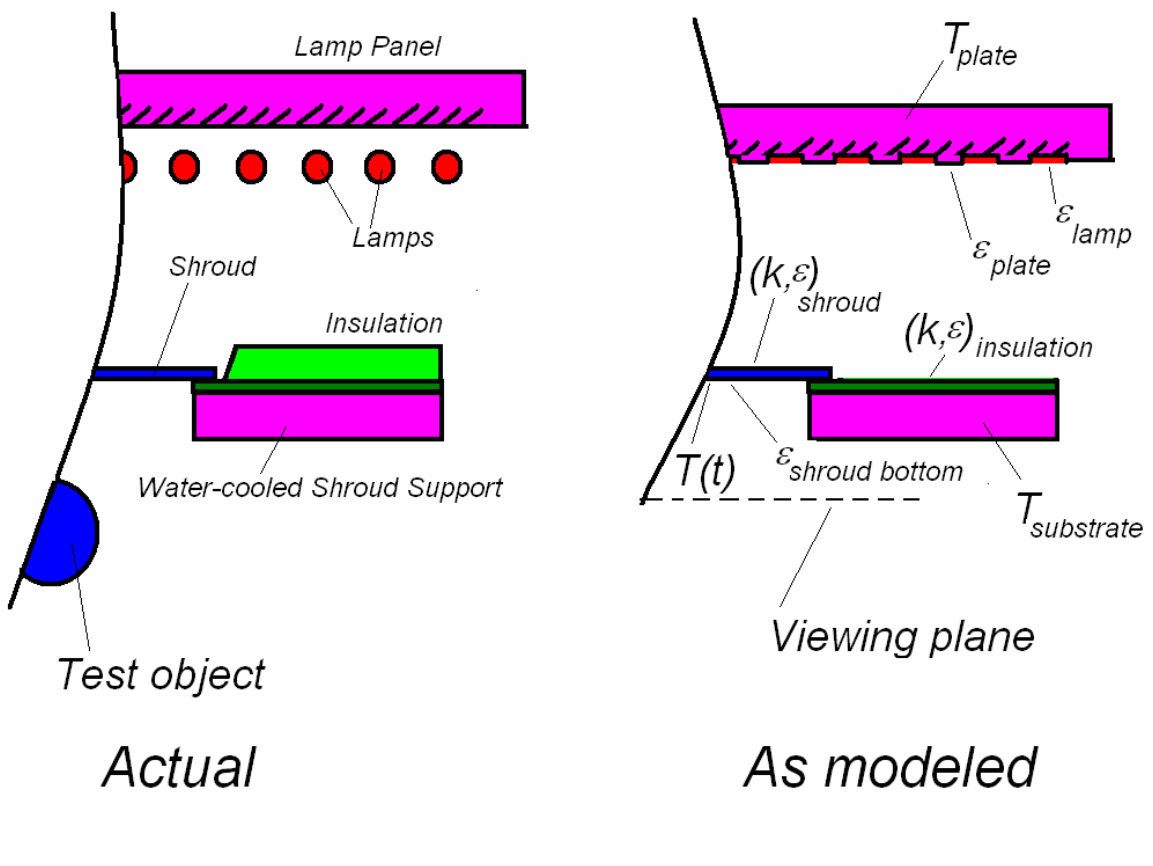

Figure 2: SPLASH schematic representation.

Figure 3 shows a color scale representation of temperature distributions calculated with the SPLASH model. The figure is a composite of two post-processing views available in SPLASH and serves to introduce the nature of the SPLASH analysis. This particular system has 407 surfaces considered in the enclosure analysis. Up to 2500 surfaces can be specified. The upper right corner of the figure shows 406 areas (one belongs to the environment) and a temperature legend. Most of the legend's colors are not present on the system because the lamp strips are much hotter than anything else in the system. At the lower left of Figure 3 the shroud is shown along with a temperature scale than spans the range of the shroud's temperatures. Notice the narrow, hot frame around the outside of the shroud. This is due to the exterior frame of areas being backed by insulation.

The GUI interface allows the user to specify which lamps are present, the number of elements along the length of a lamp, and "cell-size" for the shroud and for the insulation, and overall dimensions for the aperture, insulation and shroud. From these specifications SPLASH develops the more detailed area definitions for the whole system.

2.2 Model formulation

2.2.1 Enclosure radiation

The lamp assembly geometry was simplified by approximating lamps as strips in the same plane as the aluminum panel intervals between them. Given this simplification to

the geometry the view factor development was straightforward. All the interior surfaces defined by the geometry have no view to surfaces in their own plane and finite views to every surface in the opposite plane and the "surface" representing the environment. The appendix includes the analytical expressions used to calculate views between aligned, finite rectangles in separated, parallel planes. Given the full set of the view factors the enclosure calculation can be summarized as:

$$[H]\overline{W} = \overline{B} \tag{1}$$

where the elements of the square matrix, $[H]$, are:

$$h_{ij} = \delta_{ij} + (\varepsilon_i - 1)F_{ij} \tag{2}$$

The Kronecker delta, δ_{ij}, is one when $i = j$, otherwise zero. $\overline{W}$ is the vector of surface radiosities, and $\overline{B}$ is the vector of $\varepsilon_i \sigma T_i^4$. Given $\overline{W}$, the vector of surface heat fluxes, $\overline{q}$, is found through:

$$\{[F] - [I]\}\overline{W} = \overline{q} \tag{3}$$

where $[F]$ is the matrix of view factors and $[I]$ the identity matrix. For any given temperature state of the system, a SOR (successive over-relaxation) method was employed to find $\overline{W}$ from Eq. (1) and then the matrix multiplication of Eq. (3) yielded the corresponding fluxes. Temperature distributions were developed as follows:

1. For the zones in the lamp panel between the lamps the temperatures were specified.
2. The heat radiated per unit length along the lamps was considered to be constant and energy storage was not considered in the lamps (no ρC_p). Depending upon geometry considerations, each lamp could have a unique temperature distribution along its length at any point in time. As no energy storage is considered in the lamp segments, it is necessary to iterate within each time step to find the lamp temperature distributions consistent with the constant power per length requirement and the temperature distribution of the rest of the system.
3. All the remaining zones have associated thermal capacitance and their transient temperatures were estimated by a simple finite difference scheme.

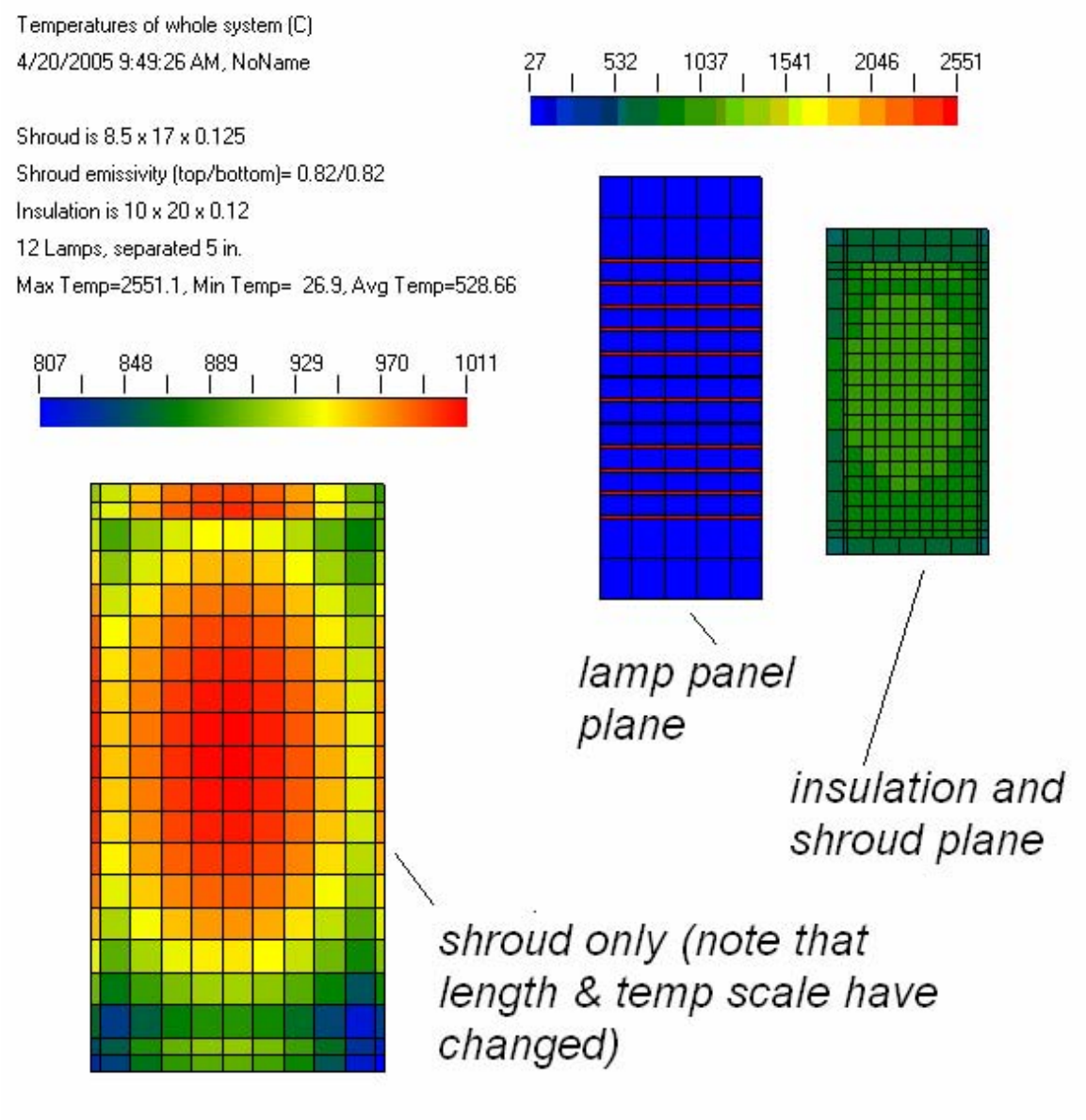

Figure 3: A typical temperature distribution for all steady radiating surfaces.

2.2.2 Q_{other}

These terms arise for conduction through the insulation, lateral conduction in the shroud, and radiation from the bottom of the shroud to the environment. These are estimated according to equations presented in this section.

The energy loss to the substrate that modifies open insulation face temperature is estimated as:

$$\frac{Q_{\text{insulation}}}{A} = \frac{\left(T^{\text{top}}_{\text{insulation}} - T_{\text{substrate}}\right)k_{\text{insulation}}}{\delta z_{\text{insulation}}} \qquad (4)$$

In Eq. (4) the storage term considers all of the thermal capacitance of the insulation layer to be at the free face temperature. Consequently, when the system operates quasi-steadily the face temperature will be the correct value when requiring the steady conduction through the insulation layer thickness to match the radiant flux. Integrating over time through an increase in the insulation temperature the storage term is over estimated because the whole layer's sensible energy has been described by the face temperature. This energy is of little interest and the performance of the rest of the system is only weakly affected by this estimate.

Energy storage in the insulation between the shroud and the substrate is not considered. In this area the energy loss through the insulation from the shroud to the substrate is estimated as:

$$\frac{Q_{\text{bottom loss}}}{A} = \left(T_{\text{shroud}}^{\text{top}} - T_{\text{substrate}}\right) \times \left[\frac{\delta z_{\text{insulation}}}{k_{\text{insulation}}} + \frac{\delta z_{\text{shroud}}}{k_{\text{shroud}}}\right]^{-1} \tag{5}$$

Figure 4 shows gridded shrouds (blue) on top of compatible grids for the insulation layer (green) for both a rectangular and a circular geometry. Lateral conduction between shroud elements in a rectangular shroud is estimated as:

$$Q_{i,j} = 2(k\delta z)_{\text{shroud}} \left\{ \Delta y_j \left(\frac{T_{i,j} - T_{i-1,j}}{\Delta x_i + \Delta x_{i-1}} + \frac{T_{i,j} - T_{i+1,j}}{\Delta x_i + \Delta x_{i+1}} \right) + \Delta x_i \left(\frac{T_{i,j} - T_{i,j-1}}{\Delta y_j + \Delta y_{j-1}} + \frac{T_{i,j} - T_{i,j+1}}{\Delta y_j + \Delta y_{j+1}} \right) \right\} \tag{6}$$

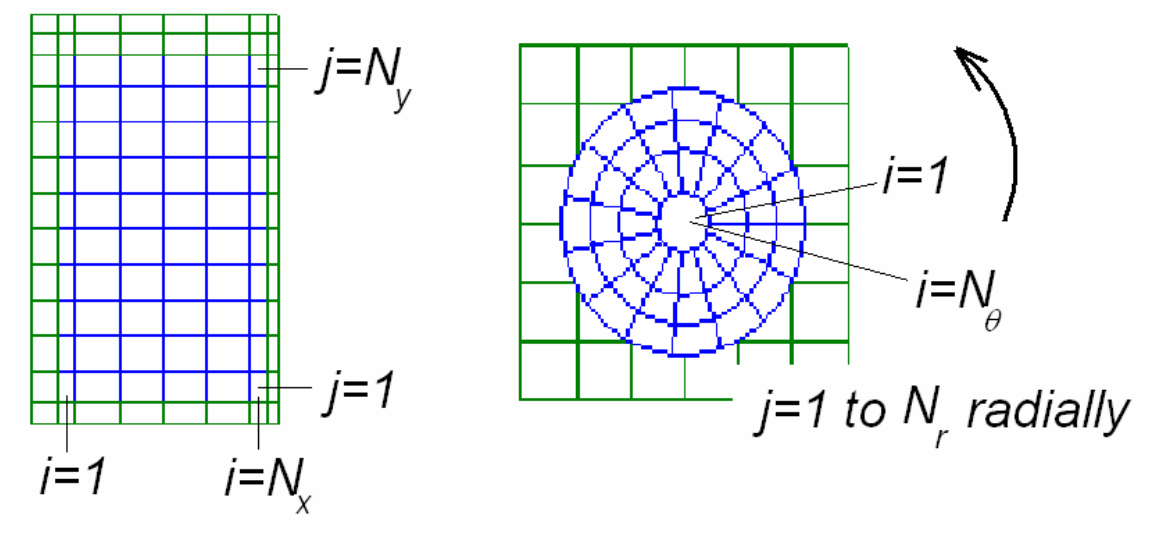

Figure 4: Schematic representation of indices on shroud for both rectangular and circular shroud cases.

Note that the finite difference terms estimating temperature gradients are written to accommodate neighboring elements of varying dimension in the direction of the gradient. The irregular size arises in SPLASH because gridlines must coincide with both the aperture through the substrate and the outside extent of the shroud. By rule, the shroud is always centered over the aperture. Appropriate terms of Eq. (6) are omitted for edge elements.

When the shroud is circular the lateral conduction is estimated by:

$$Q_{i,j} = (k\delta z)_{\text{shroud}} \left\{ \delta r_j \frac{2T_{i,j} - T_{i-1,j} - T_{i+1,j}}{\delta\theta(r_{j+1} + r_j)/2} + 2\delta\theta r_j \frac{T_{i,j} - T_{i,j-1}}{\delta r_j + \delta r_{j-1}} + 2\delta\theta r_{j+1} \frac{T_{i,j} - T_{i,j+1}}{\delta r_j + \delta r_{j+1}} \right\} \quad (7)$$

Additional logic is required to place the N_θ-th i-node before the first in gradient calculations between nodes straddling the $\theta = 0$ radial. As illustrated in Figure 4, the center element of a circular shroud is always circular. Consequently, net lateral conduction for the center element is unique. For this node there is no θ-direction conduction and the sum the radial conduction terms between the center node and the first encircling ($j = 2$) elements is applied to the center node so that energy is conserved.

In general, a temperature distribution through the shroud thickness is not resolved. However, the difference between the top and bottom shroud temperature is considered in estimating the thermal radiation from the bottom of the shroud. That is, the temperature used for the shroud bottom emissive power is:

$$T_{i,j}^{\text{bottom}} = T_{i,j} - \frac{q_{i,j}^{rad}}{(k/\delta z)_{\text{shroud}}} . \quad (8)$$

Generally, the experimental equipment is operated in shroud mode and the temperature error for determining heater power is measured at the center bottom of the shroud. SPLASH can be operated such that the preceding equation is used to indicate the shroud temperature bottom.

Alternatively, a selectable “lagging back face temperature” feature is implemented to approximately consider the temperature distribution through the shroud thickness only at that center location. If selected, this feature places two interior nodes through the shroud thickness so that a total of four (top, bottom, and two interior) temperatures characterize the temperature profile at the shroud center. When this feature is not in operation (Eq. (8) is used) there is no time delay between the response of the top and bottom shroud face temperature responses. This feature was motivated by recognition that there is delay on the order of seconds associated with thermal equilibration through typical shroud thicknesses. Consequently, additional degrees of freedom were desired to allow SPLASH to predict a control temperature that lags the top-side shroud face temperature. When selected, this feature introduces four additional transient temperatures ($T_a \ldots T_d$, shown in Figure 5) coupled to the rest of the system as follows:

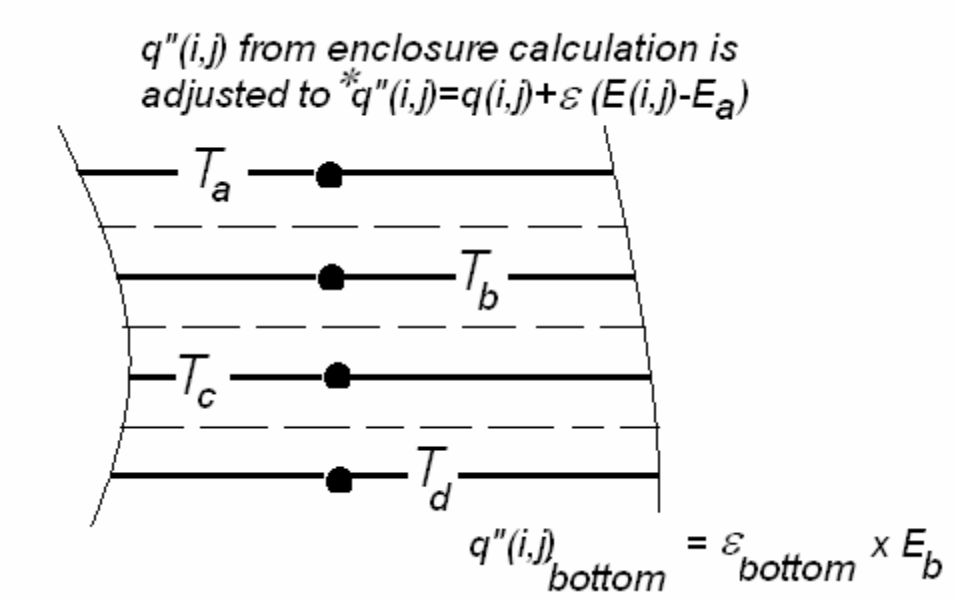

Figure 5: Four nodes through the shroud thickness.

$T_a \ldots T_d$ are to represent the distribution through the thickness at one location. As shown in the figure the local radiant flux is adjusting according to the difference between the emissive power (E_a) and that associated with the enclosure calculation. Likewise the loss of energy at the bottom of the shroud is adjusted to correspond to T_d. Simple difference operators are used to calculate the conduction flux between the layers and the time a forward finite difference operator is used to represent the time derivative to arrive at explicit expressions for each of $T_a \ldots T_d$. The limitations in the performance of this feature are not fully understood and undoubtedly depend upon operating parameters such as geometry and heating rates. Since T_a, or likewise "resolved" temperatures at other shroud locations, is not used in the enclosure analysis, it is clear that this formulation is incomplete.

2.2.3 Convection

Convection is not considered in SPLASH. Generally, the shroud temperature is sufficiently high to justify this assumption. Moreover, the shroud is generally oriented in a horizontal plane and is often considerably smaller than the lamp panel and the insulation layer in lateral extent. An extensive skirt of insulation helps to interrupt natural convective currents that form due to buoyancy effects. As fire conditions are usually simulated, radiation usually dominates. However, if use of SPLASH is extended to lower temperatures the assumption may suffer.

2.2.4 Solution Processes

2.2.4.1 Shroud Mode Transient Solution

SPLASH was principally designed to develop an estimate of temperature distribution when operating in a quasi-steady condition at the lamp power level required to maintain some specified shroud temperature. No thermal capacitance is associated with the lamps. During the transient solution of the system the steady lamp temperatures consistent with the current lamp power and the other system temperatures is continuously updated. Each time step an iterative method is used to find the corresponding lamp temperatures. Every element in the system that is part of a lamp has a net radiative flux (loss) equal to the total lamp power of the system divided by the total lamp area $\left(q_{\text{lamp}}\right)$. The temperatures corresponding to that condition are found by:

$$E_i^{new} = E_i^{old} + \left(q_{\text{lamp}} + q_{rad}\right)/\varepsilon_{lamp} \tag{9}$$

The preceding equation is evaluated for each lamp element until:

$$\sum_{heaters} \delta q_i < Q_{tol} \tag{10}$$

where Q_{tol} is a user input.

A simple forward finite difference scheme is utilized to approximate the time derivative resulting in an explicit expression for temperature at $p+1$ time step as function of that the previous time step, current energy fluxes, and thermal capacitance a given node:

$$T_{i,j}^{p+1} = T_{i,j}^{p} + \delta t \frac{\left(A_{i,j} q_{i,j} - Q_{other}\right)}{\left(V \rho C_p\right)_{i,j}} \tag{11}$$

In Eq. (11), Q_{other} accounts for any mechanism considered other than the heat fluxes associated with the enclosure calculation between the lamp plane and the shroud plane (such as conduction contributions previously discussed). In shroud mode, Equation(11) is applied to nodes representing shroud and insulation temperatures (other temperatures in the system are specified). There is no automatic time step management.[1] For typical systems a time step that is a fair fraction of one second is usually stable and results in suitable solution times. If the user chooses too small a time step the smoothness of the solution will suffer or SOR method used to solve Eq. (4) will fail and the user is advised to decrease the time step.

Figure 6 shows the simulated temperature history for the shroud control point of a typical arrangement. The user specifies a maximum temperature $(T_{\text{set point}})$, a time interval to arrive at the set point (t_{arrive}), a time (t_{reset}) at which the control algorithm is eliminated,

[1] When lagging back face temperature model is in use the finite difference operators on the temperature through the shroud thickness are the equations limiting the time step. When this feature is selected the user is coached by a pop-up window to select a time interval $< \delta z^2/(2\alpha)$, where δz is the sub-layer thickness through the shroud.

and a maximum time (t_{max}) for the analysis. Use of t_{reset} is optional. If the reset feature is selected, from t_{reset} to t_{max} the heater power is held constant at its average value for the 100 time steps preceding t_{reset}. Use of this feature is generally recommended because fluctuation in heater output is likely to introduce an undesirable lack of steadiness in the solution.

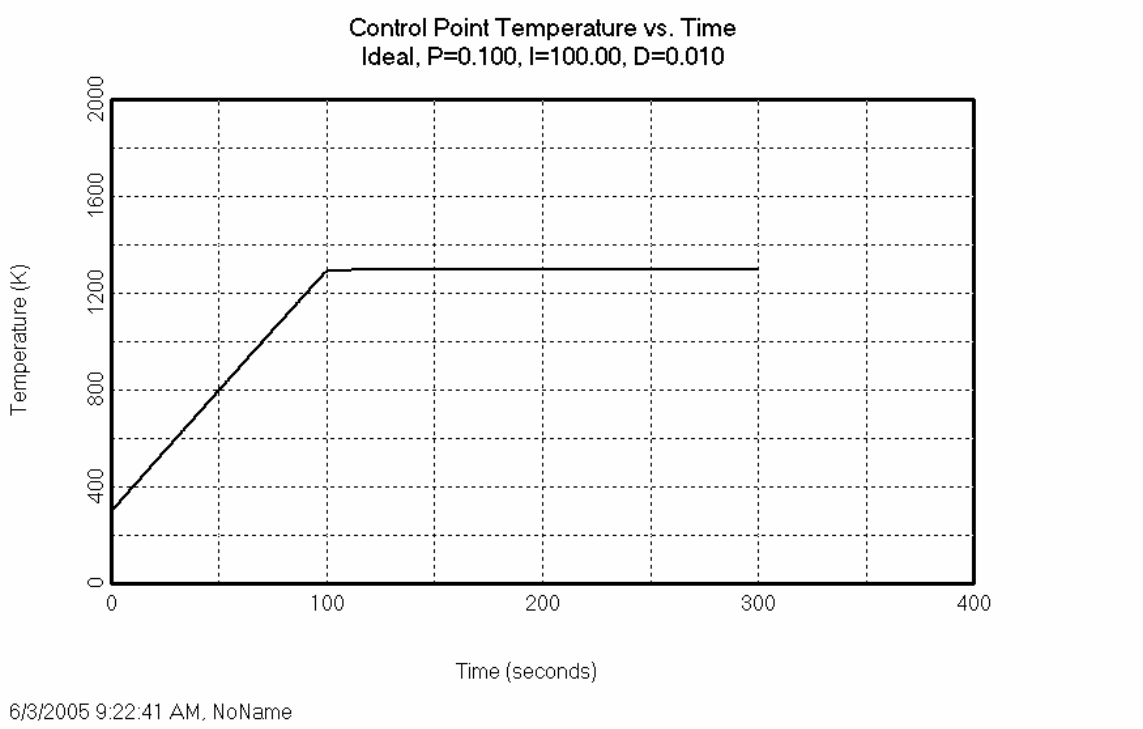

Figure 6: SPLASH predicted control point temperature versus time.

2.2.4.2 Aperture Mode Steady State

In aperture mode there is no shroud material for which to schedule temperature. As discussed earlier, in the enclosure calculation the shroud is material is represented as cold and black. The only unspecified temperatures in the system belong to the heaters and the insulation. The steady values for heater temperature are found at each state of the system as in the transient solution in shroud mode. The lamp power level is specified and there is no control system operating. In order to arrive at steady conditions a pseudo-transient is simulated for the insulation. The insulation is started at ambient temperature and "time-steps" are taken per Eq. (11) to develop the steady solution. The time step is hard-wired at a second and the volumetric thermal capacitance is fixed so that $\rho C_p = 400\ \text{kJ/m}^3$. In order to guarantee stability no temperature adjustment larger than 5K is allowed. The convergence criterion is based on the rms change of all the emissive powers in the system such that:

$$\sqrt{\frac{1}{N}\sum_{i=1}^{N}\left(1 - E_i^{p+1}/E_i^{p}\right)} < 0.001 \qquad (12)$$

2.2.5 PID Controls

Three classical proportional-integral-differential (PID) control algorithms (user selects one) are implemented to regulate the simulated heating power. These are relevant only in shroud mode. Ideal, parallel, and series definitions of the PID algorithms are defined in Ref. [3] as follows:

Ideal:

$$F = P\left\{e(t) + \frac{1}{I}\int e(t)dt + D\frac{de(t)}{dt}\right\} \tag{13}$$

Parallel:

$$F = Pe(t) + \frac{1}{I}\int e(t)dt + D\frac{de(t)}{dt} \tag{14}$$

Series:

$$F = P\left\{e(t) + \frac{1}{I}\int e(t)dt\right\}\left\{1 + D\frac{de(t)}{dt}\right\} \tag{15}$$

P, I, and D are all user-defined constants and F is the fraction of the specified maximum heater power that currently applied. $e(t)$ is the temperature error ($e(t) = SP - T_{cp}$) at the control point. For a given transient analysis, the time step is fixed and the user can also specify an integer number of analysis time steps between controller samples. The discrete series of $e(t)$ is filtered as:

$$T_f^n = 0.5T_{cp}^n + 0.25T_{cp}^{n-1} + 0.175T_{cp}^{n-2} + 0.075T_{cp}^{n-3} \tag{16}$$

where the superscripts refer to the current and successively preceding control samples. The discrete series of errors is then:

$$e(\hat{t}_n) = SP(t_n) - T_n^f \tag{17}$$

where $SP(t_n)$ is the schedule defined by user input (see Figure 6).

Given the filtered series of $e(\hat{t}_n)$, $\frac{de(t)}{dt}$ and $\int e(t)dt$ are evaluated for use in Eqs. (13-15) by a simple finite difference and trapezoid integration rule respectively. The output is "clipped" so that $0 \le F \le 1$ and only power levels between 0 and the specified maximum are allowed. Figure 7 shows "controller action" terms corresponding to the case associated with Figure 6. For this case; $P = 0.1$, $I = 100$, and $D = 0.01$. Figure 8 shows the corresponding total lamp power versus time. The results of Figure 6 through Figure 8 are pleasingly smooth. However, such results are only obtained when a small solution time step and small controller sampling interval are used.

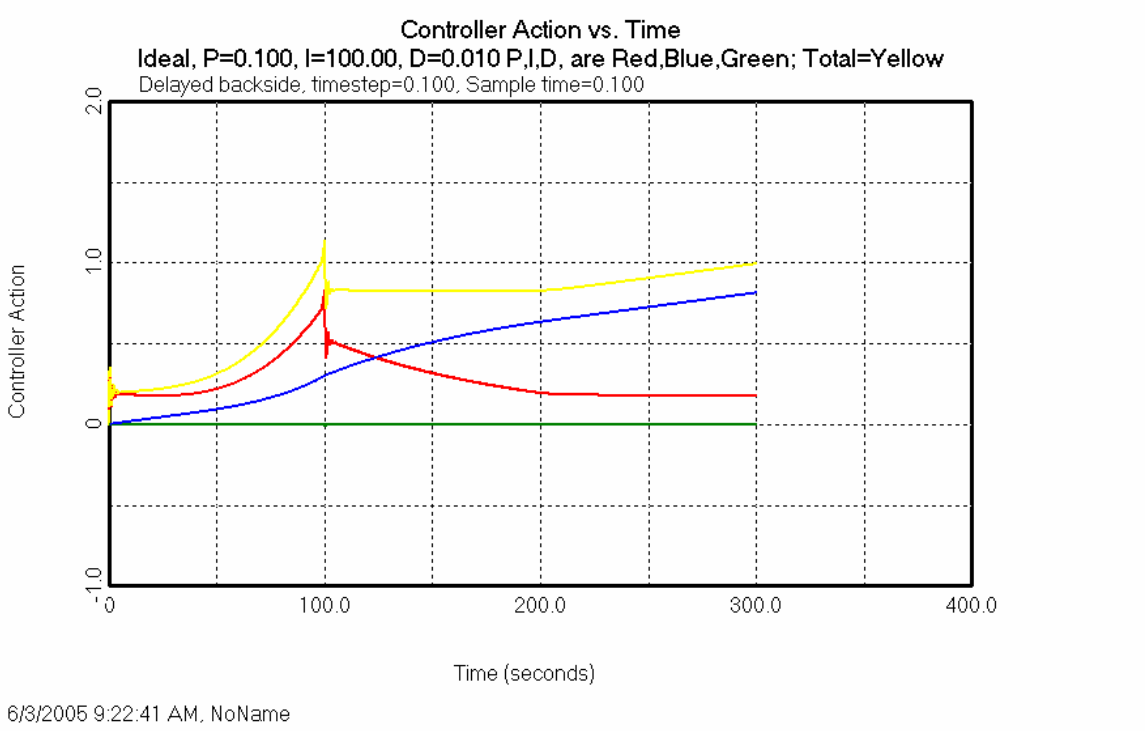

Figure 7: PID action plot.

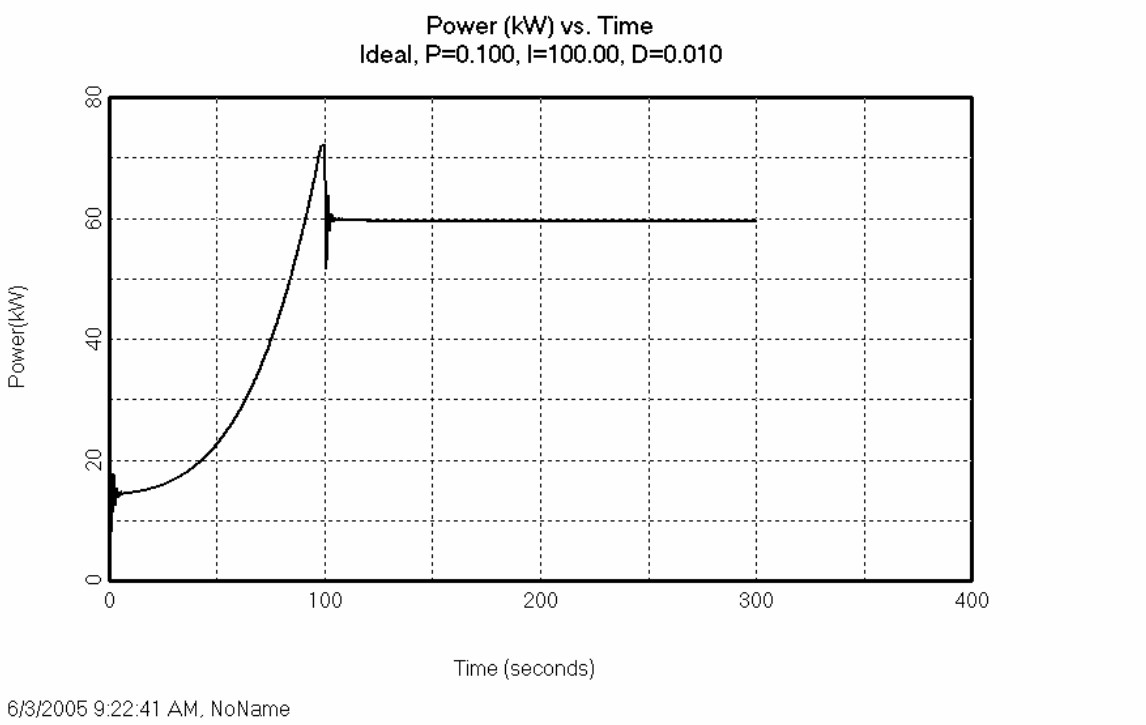

Figure 8: Simulated heater power.

The intent in implementing these algorithms was to allow SPLASH to simulate proposed control constants to eliminate some of the experimentation required to design stable heater operation. In the experimental results to be discussed there is included a plot (Figure 18) of a typical lamp panel power versus time profile and some qualitative agreement in the power plot presented in Figure 6 can be seen. However, it must be conceded that the goal of using SPLASH to test PID constants to guide test setup was not realized. The effort to simulate the actual hardware was largely stymied by the lack of information about the proprietary "black box" used to control the heaters. The difficulty may also relate to incomplete physics.

2.2.6 View Plane Calculations

As shown in Figure 2, a viewing plane is defined parallel to the shroud or aperture. After the enclosure analysis described in the previous sections is completed the model user can calculate incident radiation on a view plane. The plane is parallel to the shroud with a user-specified distance and horizontal extent. In addition to the dimensions of the view plane, the user specifies an approximate "cell-size" on the view plane. Rectangular sub-elements of the view plane are defined such that the smallest number of cells in each of the *x*- and *y*-directions is used that results in cells, at most, as large as the user specification.

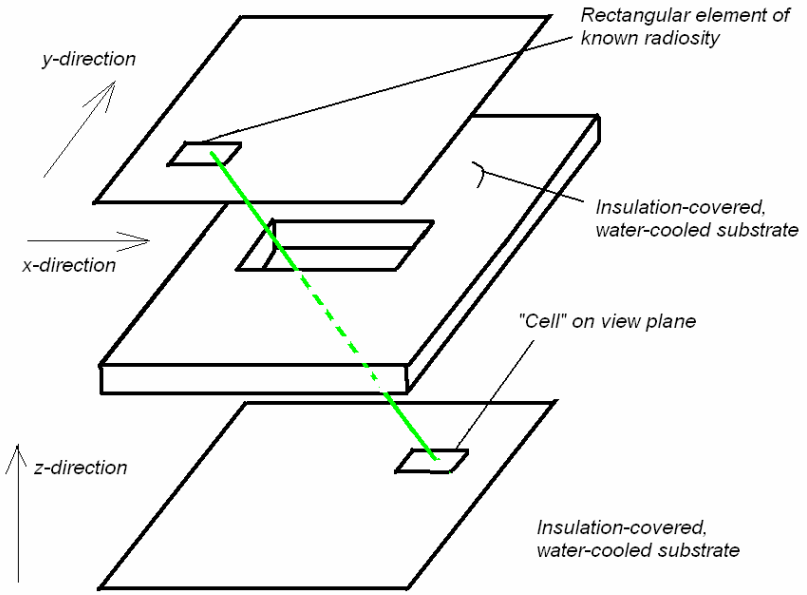

Figure 9: Schematic representation of source plane, aperture, and view plane.

Figure 9 represents the geometry used in the view plane calculations. The top plane represents the "source." In shroud mode that plane is coincident with the top face of the water-cooled substrate because the source of interest is the shroud which is supported by the substrate. In aperture mode the source plane is at the lamp level. In either case the source plane has been divided into elements and radiosities for all elements above the substrate have been calculated. Given a clean line-of-sight, the energy radiated by a differential element of area in the source plane that is incident on a differential area on the viewing plane is:

$$d^2 I = \frac{1}{\pi} \frac{W_s \cos\theta_s \cos\theta_t dA_s dA_t}{(R_{s-t})^2} = \frac{1}{\pi} \frac{W_s Z^2 dA_s dA_t}{(R_{s-t})^4} \tag{18}$$

In the preceding equation the cosine operates on the angle between the surface normal and the line of sight under consideration. W_s is the radiosity at the source. In the rightmost portion of Eq. (18) the cosines have been replaced by ratio of the vertical separation to the slant distance (exploiting the fact that the surfaces we consider are always parallel). The incident irradiance on a finite element in the viewing plane is then calculated as:

$$I_{l,m} = \frac{1}{\pi A_{l,m}} \sum_{S} \sum_{dA_s} \sum_{dA_t} g(R_{s-t}) \frac{W_s Z^2 dA_s dA_t}{(R_{s-t})^4} \tag{19}$$

In the preceding equation $\sum_{S}$ represents summing over all of the finite areas of the source plane. In shroud mode, $\sum_{S}$ accounts for all of the area on the bottom of the shroud within the aperture. In aperture mode, $\sum_{S}$ accounts for all the lamps and the intervening areas in the same plane.

$\sum_{dA_s}$ and $\sum_{dA_t}$ represent summations on sub-areas of the source area and the cell on the viewing plane respectively. Each of these summations represents increments in two directions (x and y or r and θ). The number of increments is chosen so that dA_s and dA_t are not larger than 0.25".

Finally, $g(R_{s-t})$ represents the test function to determine whether the line of sight for the current path, R_{s-t}, is eclipsed. In shroud mode, if R_{s-t} intersects the plane at the bottom of the substrate within the confines of the aperture then $g(R_{s-t}) = 1$, otherwise $g(R_{s-t}) = 0$. In aperture mode, if R_{s-t} intersects both of the planes at the top and bottom of the substrate within the confines of the aperture then $g(R_{s-t}) = 1$, otherwise $g(R_{s-t}) = 0$.

Figure 10 is an example of the irradiance calculation on the viewing plane for an unlikely aperture mode geometry. The top part of the figure shows SPLASH's schematic representation of the system. A slit-shaped aperture sits 5" below the lamp plane. The viewing plane is 4" below that. Notice that the "image" of the lamps on the viewing plane is reversed appropriately for the slit aperture of this problem.

Figure 11 shows a view plane result for a shroud mode calculation. The results shown in Figures 2, 5, 6, 7, and 10 are all from the same SPLASH analysis.

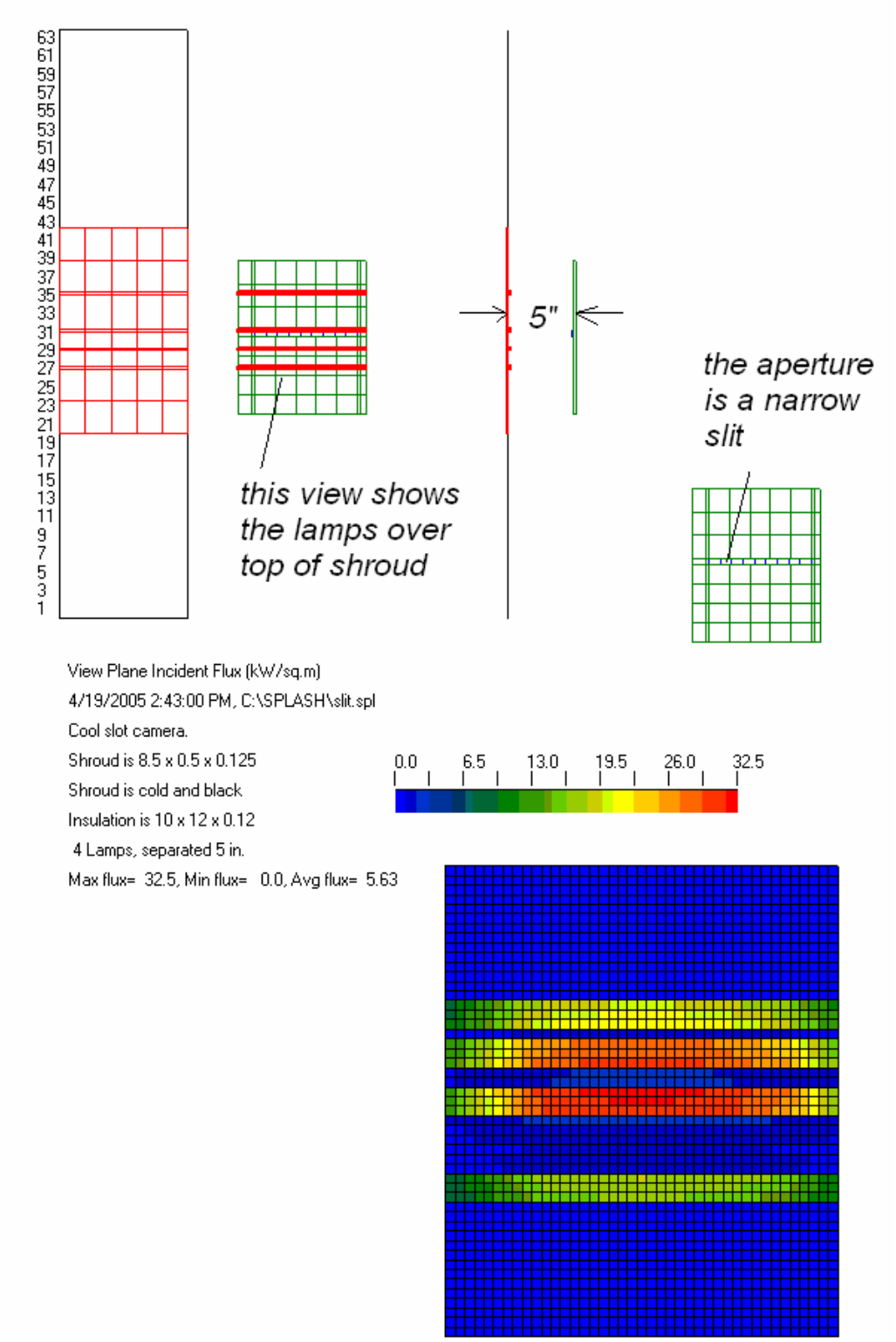

Figure 10: View plane results for a slit-shaped aperture.

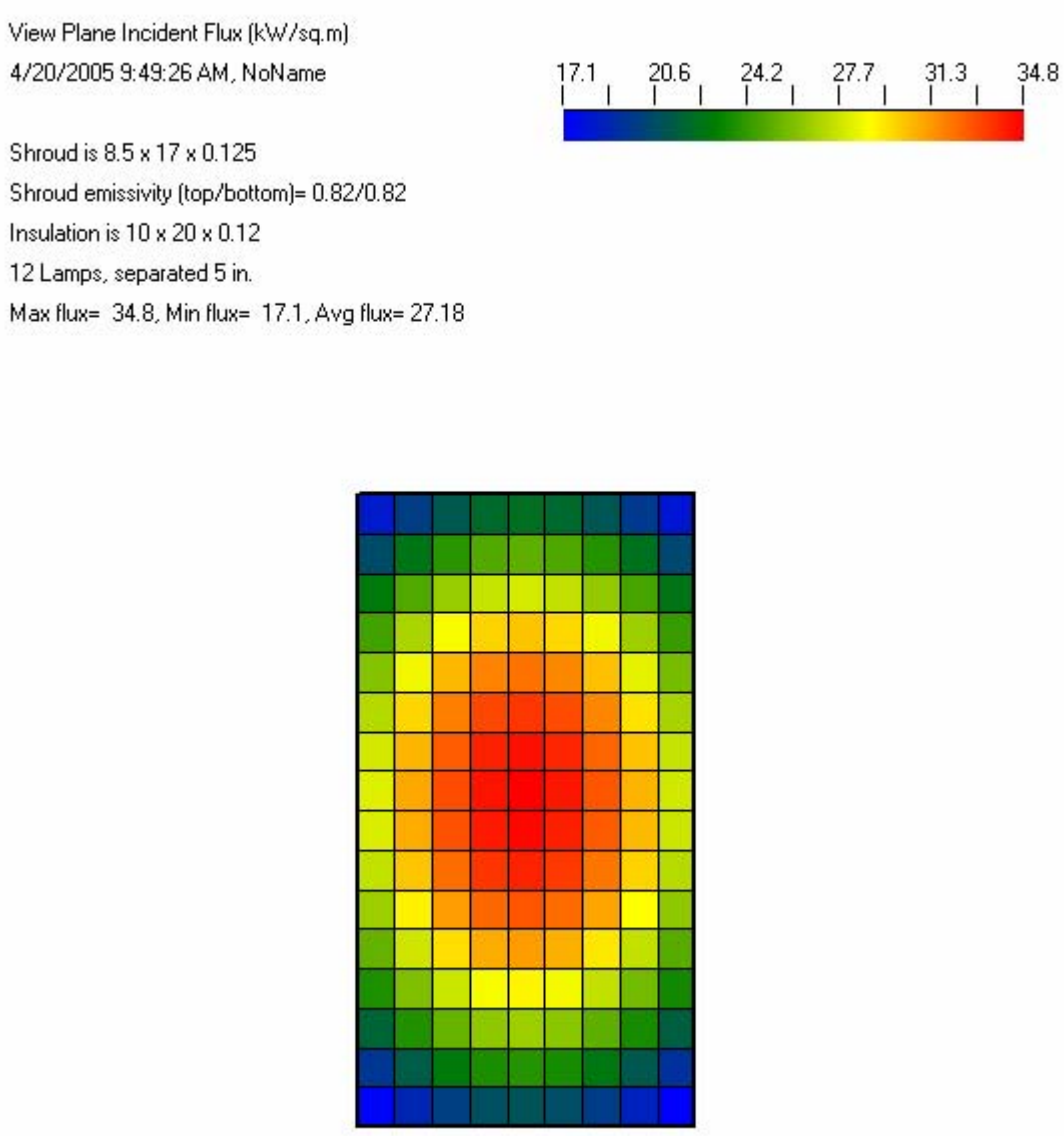

Figure 11: View plane result for shroud mode.

3 Experimental Validation

A useful and early version of SPLASH was made available approximately May of 2004. The summer of 2004 provided an opportunity to perform testing to demonstrate that SPLASH could produce useful estimates. Development of SPLASH's view plane and the aperture mode occurred after the experimentation to be described in this section.

The innumerable variations in geometry, material properties, and control temperatures and schedule can not be affordably and exhaustively tested. This section gives a detailed description of tests designed to vary important parameters and characterize SPLASH's performance in terms of shroud temperatures at quasi-steady conditions.

3.1 Design of Experiments

Experiments using a flat panel array were conducted to determine the accuracy of the SPLASH formulation. In order to identify potential flaws and learn the sensitivity of the model, five parameters (factors) were chosen as experimental variables. These five factors are listed in Table 1, each with two settings.

Table 1: Parameters used in tests.

Factor	Setting 1	Setting 2
A) Shroud geometry	Circular	Rectangular
B) Lamp location	Offset	Centered
C) Panel height	4 in	8 in
D) Insulation over-lap	0.25 in	0.50 in
E) Temperature	600 °C	1000°C

Unfortunately, a miscommunication/misunderstanding existed during the execution of these tests regarding the "insulation overlap." Figure 12 shows images of the circular shroud that was tested with ½-inch insulation overlap which was interpreted to mean that the radius of the circular hole through the insulation was ½-inch less than that of the hole through the water-cooled substrate. The SPLASH model does not allow the specification of a hole-size through the insulation that does not match that through the substrate (refer to Figure 2 and Ref. [2]). Consequently, in this overlap region the test specimens actually radiated to the environment while the SPLASH analyses represent the bottom side of the insulation in that same area as conducting to the water-cooled substrate. It's difficult to predict the effect of the error. Contact resistance is not represented between the insulation layer and the water-cooled substrate or between the shroud and its supporting insulation. If the actual contact resistance is sufficiently high, the radiation away from the overlap insulation to the environment may constitute a boundary condition that is much like the intended boundary so that the measured result may not have been changed much by the error. Since the bottom side of the insulation in the SPLASH model is specified at the cooled substrate temperature, the model should predict temperatures lower than were actually experienced in the shroud material over the overlap region. Note that this area will generally not be included in the assessment of model accuracy to follow because it is out of sight of the thermal imaging used. However, since there is lateral conduction in the shroud (both real and modeled), the model prediction for this region will affect the shroud material adjacent to it. That is, we expect the result of the model to exhibit suppressed temperatures at the perimeter of the imaged temperature field.

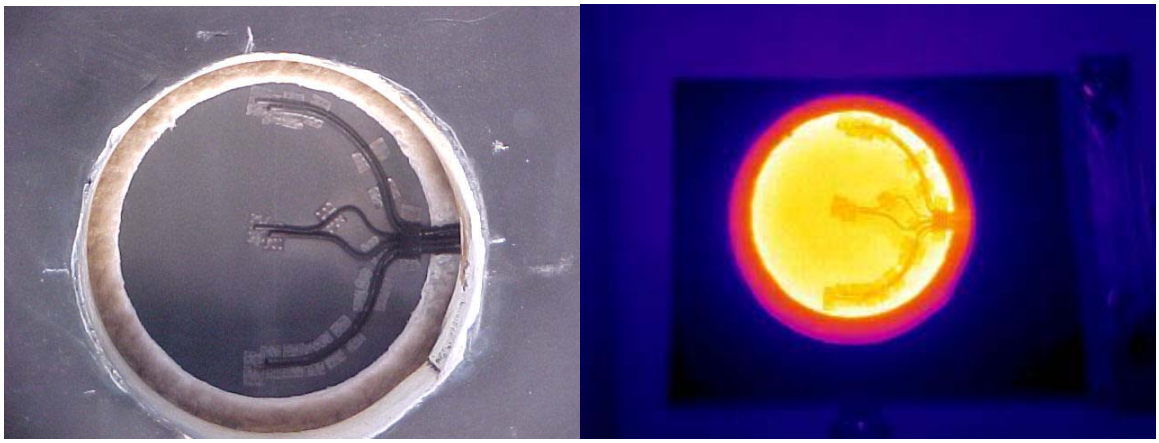

Figure 12: Images of cool and heated circular shroud as tested with ½-inch insulation overlap.

To limit the time and resources required for these experiments, a one-quarter fraction of a 2^k experimental design was chosen. This experimental plan requires 8 experiments, each conducted twice. The experimental test plan is presented in Table 2.

Because it was not known how repeatable the tests were, replicate tests were conducted. This reduced the number of unique parameter sets that could be tested by a factor of two but increased confidence in the data. Table 2 has been sorted the RMS temperature error observed by the process to be described in the following sections. Duplicate tests are indicated by the same number and differ by the 'a' and 'b'. For example 1a and lb are for the same test conditions. For each experiment conducted, a corresponding analysis was completed using SPLASH. For several instances in Table 2 the replicate tests are adjacent rows, which is an indication of the tests repeatability. Where the row order departs from expectation the difference in observed RMS temperature error for replicate tests is less than 2°C.

3.2 Radiant Heat Experiments

Lamps were installed on the lamp panels in two configurations, centered and offset. The centered configuration consisted of 21 lamps centered over the shroud. A schematic representation is shown in Figure 13. The lamps are shown in red (Lamp Level), insulation in green (Shroud Level), and shroud in blue (Shroud Level). A side view showing the separation distance between the lamps and shroud is also provided.

Since the lamps are positioned 0.72 inches apart, approximately four lamps were positioned past the end of the rectangular shroud, and all but 5 lamps were beyond the edges of the circular shroud.

Figure 14 is an image of the offset lamp configuration. Note the size of the rectangular shroud beneath the lamps. Also note the center position labeled on the lamp panel.

Table 2: One-quarter fraction of the 2^k experimental test plan.							
Test	Order	Shroud Type	Lamp Config.	Separation in.	Insulation Overlap in.	Temperature °C	RMS of Temp Error °C
5a	9	Rectangular	Centered	4	0.25	600	4.59
4a	7	Circular	Centered	8	0.5	600	9.72
8a	15	Rectangular	Centered	8	0.25	1000	10.29
4b	8	Circular	Centered	8	0.5	600	10.47
5b	10	Rectangular	Centered	4	0.25	600	11.47
8b	16	Rectangular	Centered	8	0.25	1000	11.95
7b	14	Rectangular	Offset	8	0.5	1000	13.45
3b	6	Circular	Offset	8	0.25	600	13.86
3a	5	Circular	Offset	8	0.25	600	14.46
7a	13	Rectangular	Offset	8	0.5	1000	15.31
6a	11	Rectangular	Offset	4	0.5	600	15.92
6b	12	Rectangular	Offset	4	0.5	600	16.02
1a	1	Circular	Centered	4	0.5	1000	19.5
1b	2	Circular	Centered	4	0.5	1000	22.9
2b	4	Circular	Offset	4	0.25	1000	29.29
2a	3	Circular	Offset	4	0.25	1000	31.81

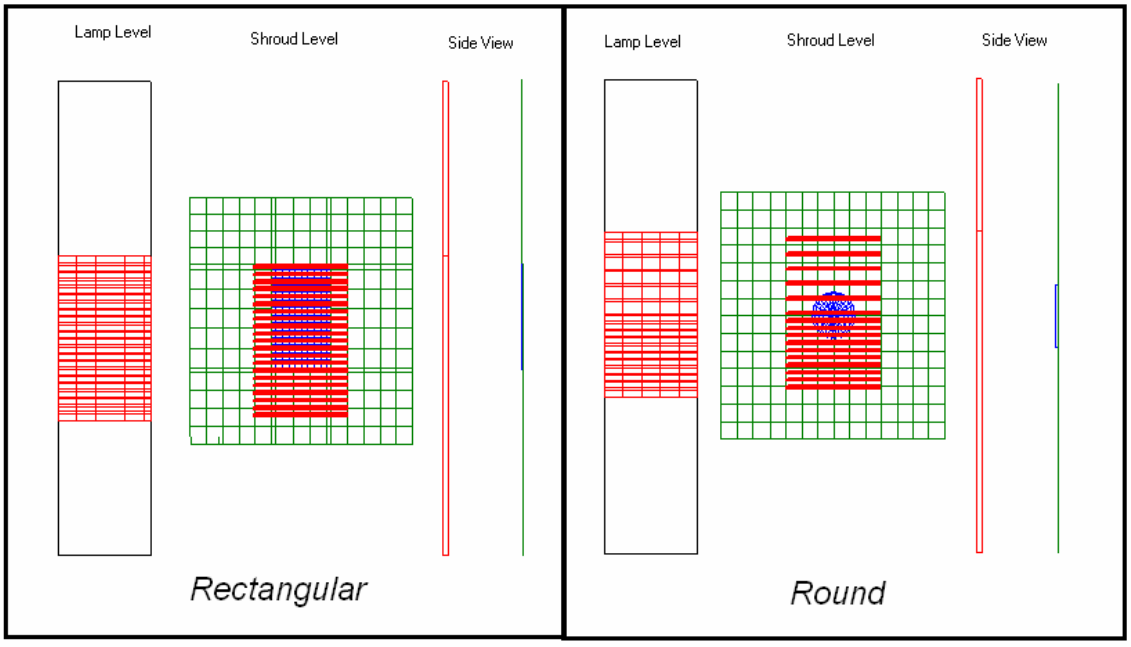

Figure 13: SPLASH test setup schematics for offset lamps with rectangular and circular shrouds.

Figure 14: Image of offset lamp configuration.

The shrouds used were a 4.75” diameter 0.125” thick circular inconel shroud and a 10.5” × 6.5” × 0.125” rectangular inconel shroud. The shrouds were painted black with Pyromark® 2500 paint. Pyromark is high-emissivity paint capable of withstanding temperatures up to ~ 1100 °C. The shrouds were dried and cured according to the manufacturer’s instructions.

Each shroud was instrumented with type k thermocouples. The thermocouple placement for the rectangular shroud is shown in Figure 15 and for the circular shroud in Figure 16. Two sizes of thermocouples were used: 0.063 inch and 0.040 inch thermocouples. The smaller thermocouples are more accurate, but tend to fail at temperatures above ~1000°C. Figure 17 is a photograph of the circular shroud.

To adjust the thermocouple readings to incorporate conduction and convection losses thermocouples were instrumented on the top and bottom of the shroud. By averaging the measurement on the top and bottom of the shroud a mean shroud temperature could be deduced (Ref. [4]). The temperature errors associated with the thermocouple readings have been studied [4] and an uncertainty of about 0.6% of the absolute temperature reading is used in this study. Considering TC error, mounting, data acquisition system, and installation errors typical total measurement errors for similar systems have been estimated [5] as 2-3%.

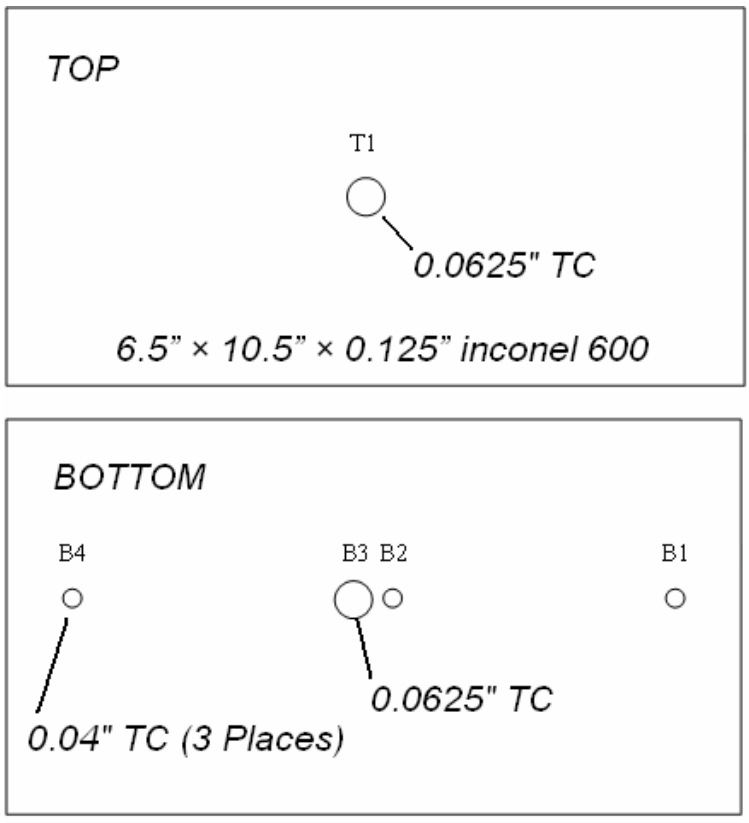

Figure 15: Top and bottom of instrumented rectangular shroud.

Because of uncertainty in the thermocouple readings due to the finite size of the thermocouple required for durability at high temperatures, a two color pyrometer (Micron Model M668) was also used to measure temperature on the bottom surface of the shroud. This pyrometer read the temperature on the bottom of the shroud just off the tip of the center thermocouples. With proper positioning, the reading from the pyrometer agreed well with the average of top and bottom thermocouples at the center as shown in Table 3.

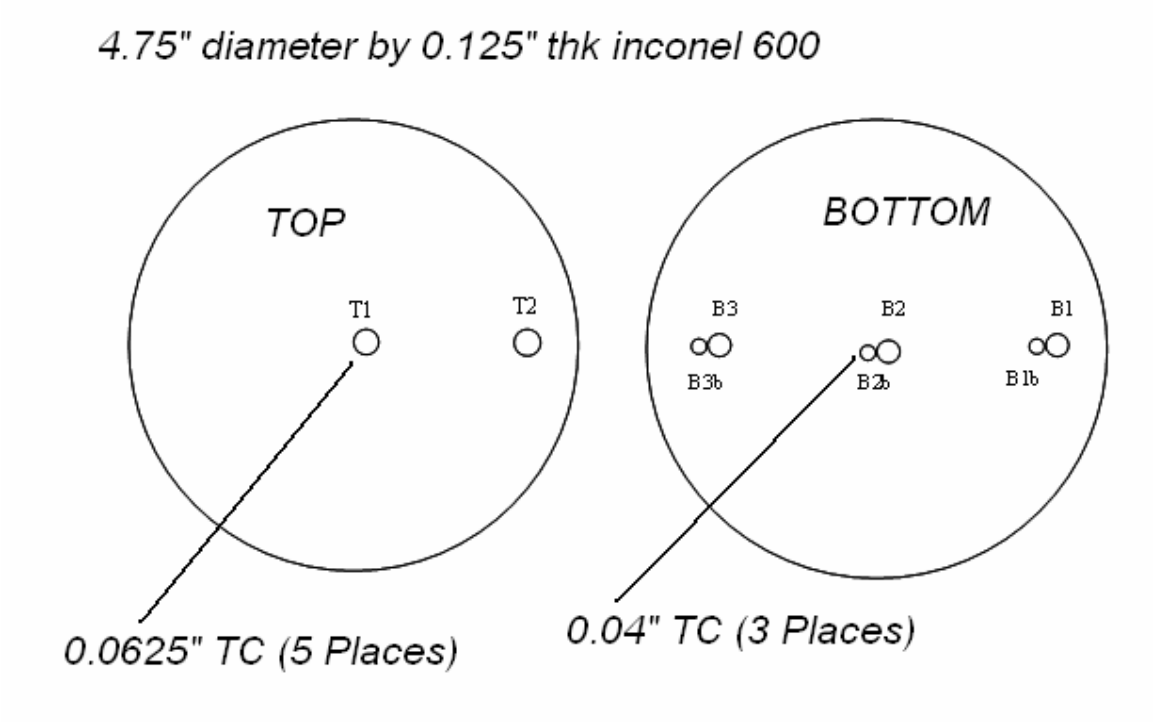

Figure 16: Top and bottom of instrumented circular shroud.

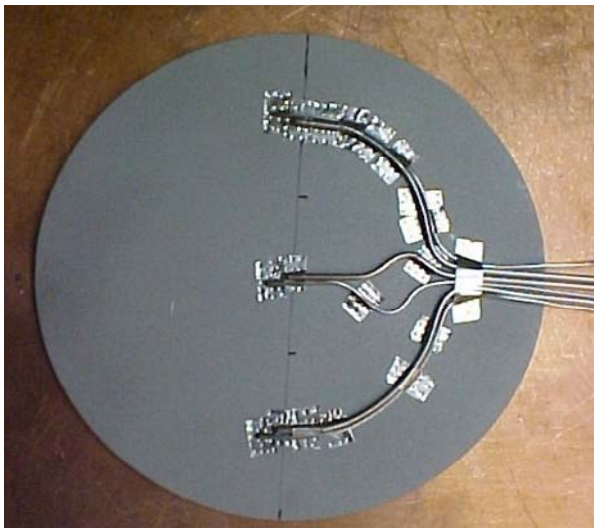

Figure 17: Image of circular shroud bottom.

Table 3: Pyrometer and average center top and bottom thermocouple reading comparison.							
Test	top/bot avg (°C)	dev ± (°C)	TC uncertainty ± (°C)	pyro avg (°C)	dev ± (°C)	error avg (°C)	dev ± (°C)
1a	1035.5	4.3	7.9	1033.6	1.4	2.5	1.4
1b	1034.2	5.5	7.8	1063.7	4.4	29.5	2.2
2a	1065.2	4.5	8.0	1061.0	5.2	4.2	0.9
2b	1067.8	4.7	8.0	1064.0	5.2	3.8	1.1
3a	621.1	2.7	5.4	624.4	2.8	3.3	0.8
3b	622.0	1.8	5.4	624.8	2.2	2.8	0.8
4a	617.6	1.2	5.3	637.6	1.4	20.0	0.6
4b	618.1	0.7	5.3	636.9	1.0	18.9	0.6
5a	601.3	1.7	5.2	-	-	-	-
5b	601.3	1.6	5.2	596.0	1.6	5.3	0.7
6a	600.2	1.5	5.2	593.8	1.3	6.4	0.6
6b	599.6	1.8	5.2	592.2	1.9	7.4	0.6
7a	997.4	1.7	7.6	996.9	2.1	2.8	1.4
7b	995.9	1.5	7.6	998.5	1.4	2.7	0.8
8a	1052.9	1.1	8.0	1052.9	0.9	0.5	0.3
8b	1054.9	1.7	8.0	1050.5	2.2	4.4	0.8
*The pyrometer was accidentally turned off during test 5a.							

In these experiments the shroud temperature is initially linearly ramped from ambient temperature to the desired steady temperature. The steady temperature was held for only five minutes. Since no object was interacting with the shroud, steady state was reached quickly. Figure 18 shows the measured power and temperature for Test 8a. The control thermocouple is located on the bottom side of the shroud. When running the corresponding SPASH tests, the actual shroud temperature at the center calculated from the top/bottom average was used, not the control temperature.

To evaluate the accuracy of shroud temperature predictions by SPLASH, an infrared camera was used to measure spatial temperature distributions on the bottom surface of the shroud. An accurate estimate of surface emissivity in the wavelength interval of the infrared camera is necessary to convert intensities into useful temperatures. This

calculation was done using the infrared camera's accompanying software. The emissivity was calculated by comparing the measured intensity with the known temperature from pyrometer and thermocouple data. The emissivity was calculated at each thermocouple location. Ideally all emissivity values calculated on the shroud should agree; this was not always true. If discrepancies occurred, the emissivity calculated at the control thermocouple was used. Emissivity values are shown in Table 4.

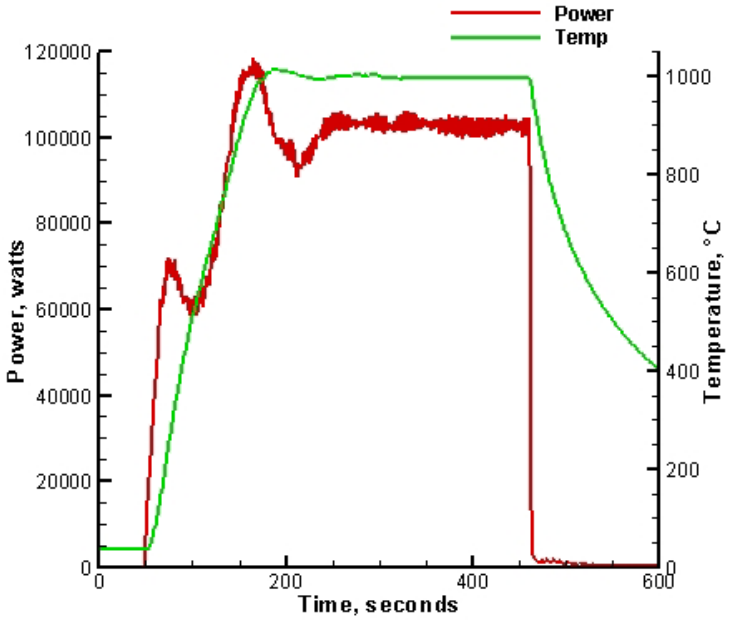

Figure 18: Temperature and power ramps from test 8a.

Table 4: Emissivity values calculated using the IR camera software from the pyrometer and thermocouple average temperatures.	
Test	**Emissivity**
Test 1a, 1b, 2a, 2b, 3a, 3b, 4a, 4b, 6a	0.96
Test 5a, 5b	0.97
Test 6b	0.92
Test 7a*, 7b, 8a, 8b	0.73
*At high temperatures the black paint baked off of the shroud, revealing the unpainted oxidized inconel surface, thus the lower emissivity values for tests 7a – 8b.	

3.3 Infrared Image Analysis

In order to compare the infrared camera images with the temperatures predicted by SPLASH, the mesh used in SPLASH needed to be mapped onto the pixel data from the camera. Knowing the dimensions of the shroud it was assumed that the pixels were evenly distributed. It was thus vital that the camera was positioned perpendicular to the shroud so that a keystone effect was avoided. The camera software also allowed image cropping. Cropping the image as accurately as possible, so as to capture only the shroud surface, allowed the exact dimensions of the image to be used to calculate the corresponding actual location on the shroud of each pixel in the bitmap file (Figure 19).

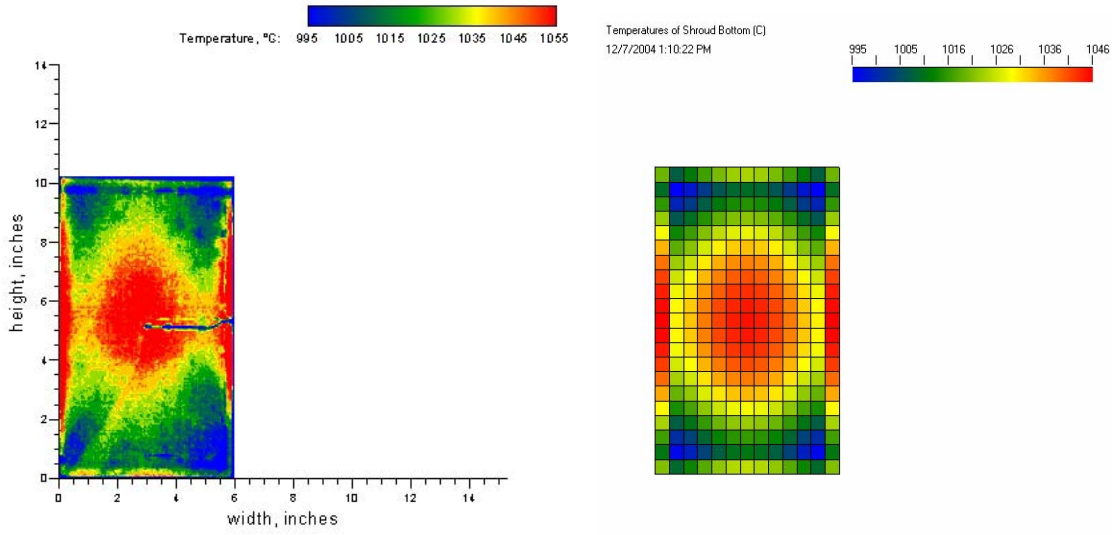

Figure 19: Comparison of an IR camera image of the bottom of the rectangular shroud (left), and a SPLASH generated temperature profile of the bottom of the same shroud (right).

The pixels were mapped onto the SPLASH mesh via a C++ program. The measured temperature at each pixel was compared with the temperature calculated at that location. The average difference between the measured temperature and the calculated temperature within each element was then calculated. The root-mean-square of the elemental error was then calculated and used to determine of how the model compared with the experiment. Images of the pixel by pixel error were also generated to see the spatial nature of the error (Figure 20). The white portions represent large errors caused by the lower temperatures of the thermocouple leads.

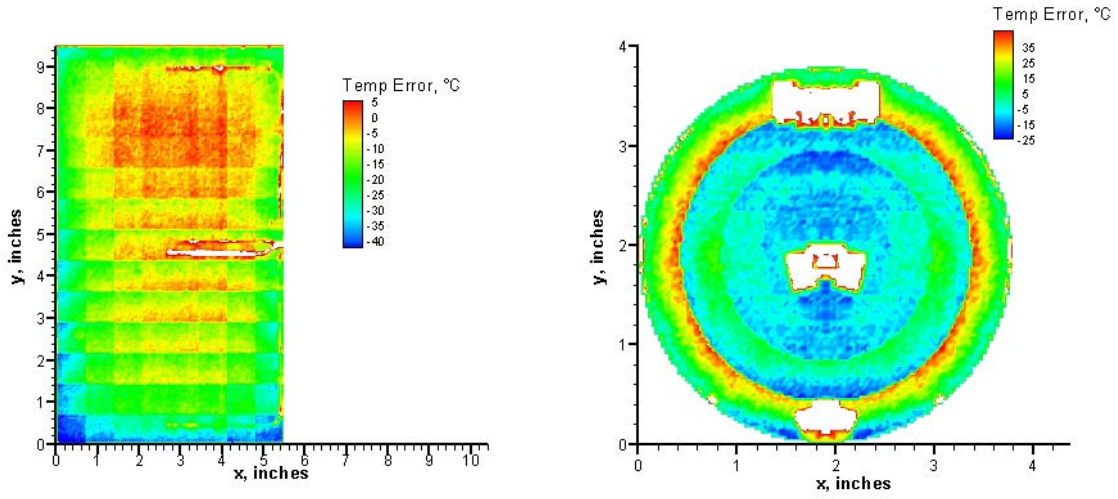

Figure 20: Comparison plots of predicted and actual temperature distributions on the bottom surface of the shroud.

3.4 Test Results

The steady-state solution was of principal interest in our analysis. Thus, IR images, TC data and pyrometer data were collected during the steady portion of the control experiment. The standard deviation of the thermocouple readings for the steady portion of the experiments was less than 5°C (Table 3). The temperatures taken from TC and pyrometer data as well as the emissivity and IR camera measured temperatures are listed in Table 5. Refer to Figure 15 and Figure 16 for thermocouple placement information.

The emissivity values were calculated based upon both the average top and bottom center TC readings and the pyrometer reading. When these two values did not agree, a temperature between the two was often used. Thus, for an uncertainty analysis, we must include the TC uncertainty, the averaging process uncertainty, the pyrometer uncertainty and the emissivity non-uniformity on the shroud's bottom surface. However, the control temperature in SPLASH was set equal to that of the emissivity corrected IR camera image at the center of the shroud. Thus, only the uncertainty in the emissivity influenced uncertainties in the error calculations. All other uncertainties in TC readings, averaging techniques or pyrometer readings do not contribute.

The root mean square of temperature error for each test is listed in the last column of Table 3. In order to determine which design variables were affecting the temperature error, a statistical analysis of the results was conducted. This was done using Minitab software (Ref. [6]). The results are shown in Figure 21 and Figure 22.

Figure 21 shows those variables whose variation is within some tolerance of a normal distribution (black circles) and those variables whose variation was beyond that found in a normal distribution (red squares). The variables whose variation was not within a normal distribution have a significant effect on how well SPLASH replicates the shroud temperature. Interactions between variables were also analyzed.

Figure 21 shows that three variables significantly affected SPLASH's ability to accurately predict the temperature of the shroud:

Lamp position

Shroud type

Lamp height

The poorest results were obtained with a circular shroud at 1000°C. For that shroud, the offset lamp position was worse than the centered lamp position. The best results were obtained with centered lamps at low temperatures.

Figure 22 shows the effects of each variable in the tests. Note that the larger effects match those predicted in the previous figure.

Detailed maps of differences between the SPLASH calculation and the corresponding experiments are shown in Figure 23 and Figure 24 for each set of parameters tested for round and rectangular shrouds respectively. The reader is reminded that the offset lamp geometries are depicted in Figure 13 and that the offsets are very significant. For the smaller lamp separation distance, the horizontal displacement of the shroud relative to being centered was three lamp separations. The angle between a ray connecting the shroud center to the lamp array center and the surface normals was ~70°.

For the circular shroud (Figure 23), the error comparison shows sharp changes occurring in concentric circles. The theoretical model assumes that individual area elements in the enclosure analysis are isothermal. Consequently, the edges are well-defined in this error expression as the data varies more uniformly. In these results there are four distinct radial positions in the SPLASH models. In the experimental results the leads (prominent in Figure 17) produce very significant errors compared to the regions away from the leads. To avoid these, the views in Figure 23 are constructed using IR data from the half of the shroud not heavily covered by leads (note the symmetry about the vertical bisector). The temperature scales vary in the four plots and regions coinciding with TC locations are "saturated." Notice that a large part of the error range typically occurs on a radial traverse across one position. The implication is that this error can be reduced by using smaller elements in the SPLASH model. For the centered lamp arrays (more typical of operations) most of the area associated with largest errors occurs at the inner edge of the outside annulus of area elements.

Table 5: TC, Pyrometer, and IR Camera Temperatures and calculated emissivity.

Test	T1	T2	B1	B1b	B1 IR	B2	B2b	T1 – B2 avg	B2 IR	B3	B3b	T2 – B3 avg	B3 IR	pyrometer	emissivity
1a	1070	1092	1040	1050	1075	998	1034	1034	1040	1076	1092	1084	1110	1031	0.96
1b	1064	1085	1043	1057	1097	1000	1040	1032	1060	1080	1099	1082	1120	1061	0.96
2a	1124	1101	1054	1067	1098	999	1037	1062	1060	1013	1025	1057	1060	1057	0.96
2b	1132	1113	1047	1062	1111	1000	1042	1066	1071	1018	1033	1066	1071	1061	0.96
3a	640	635	619	626	644	597	619	619	626	602	612	618	629	623	0.96
3b	643	639	622	630	644	599	620	621	625	608	618	623	626	623	0.96
4a	640	654	624	633	651	602	622	621	622	628	642	641	645	640	0.96
4b	636	649	623	632	648	599	619	618	626	625	638	637	648	636	0.96

Test	T1	B1	B1 IR	B2	B3	T1 – B3 avg	B2 IR	B4	B4 IR	pyrometer	emissivity
5a	616	576	587	599	589	603	602	580	583	No data	0.97
5b	616	576	587	599	589	603	602	578	581	596	0.97
6a	619	622	635	600	585	602	602	552	557	596	0.96
6b	615	623	638	598	585	600	600	551	560	594	0.92
7a	1043	1015	1023	1000	953	998	998	956	940	999	0.73
7b	1043	1005	1014	999	948	995	995	949	931	999	0.73
8a	1108	1004	1015	1046	998	1053	1053	1010	1012	1053	0.73
8b	1110	1006	1014	1046	999	1054	1055	1009	1011	1051	0.73

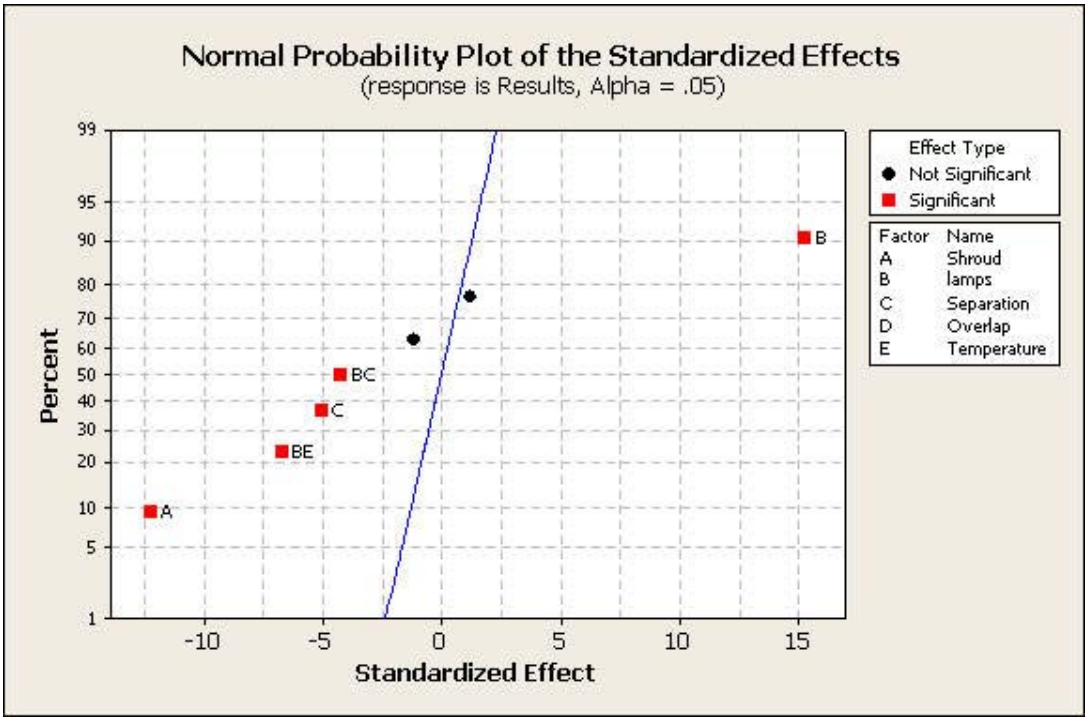

Figure 21: **Minitab summary of SPLASH variable sensitivity.**

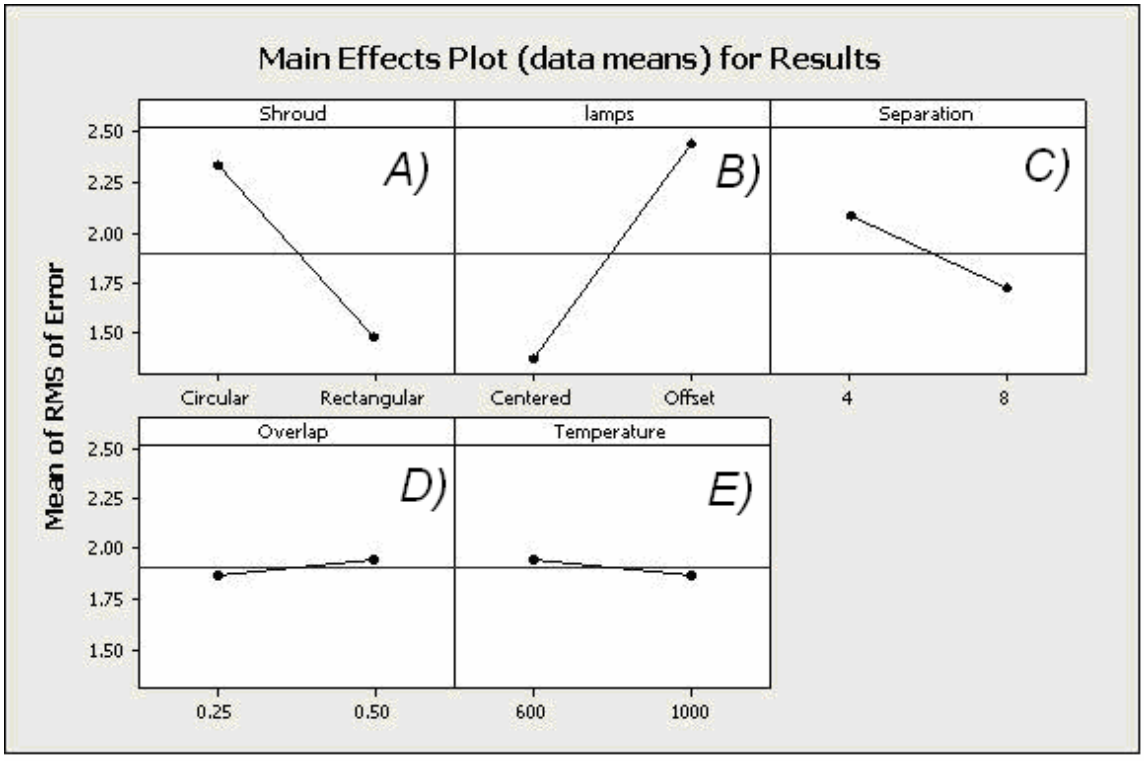

Figure 22: Minitab summary of the effects of each variable in SPLASH tests.

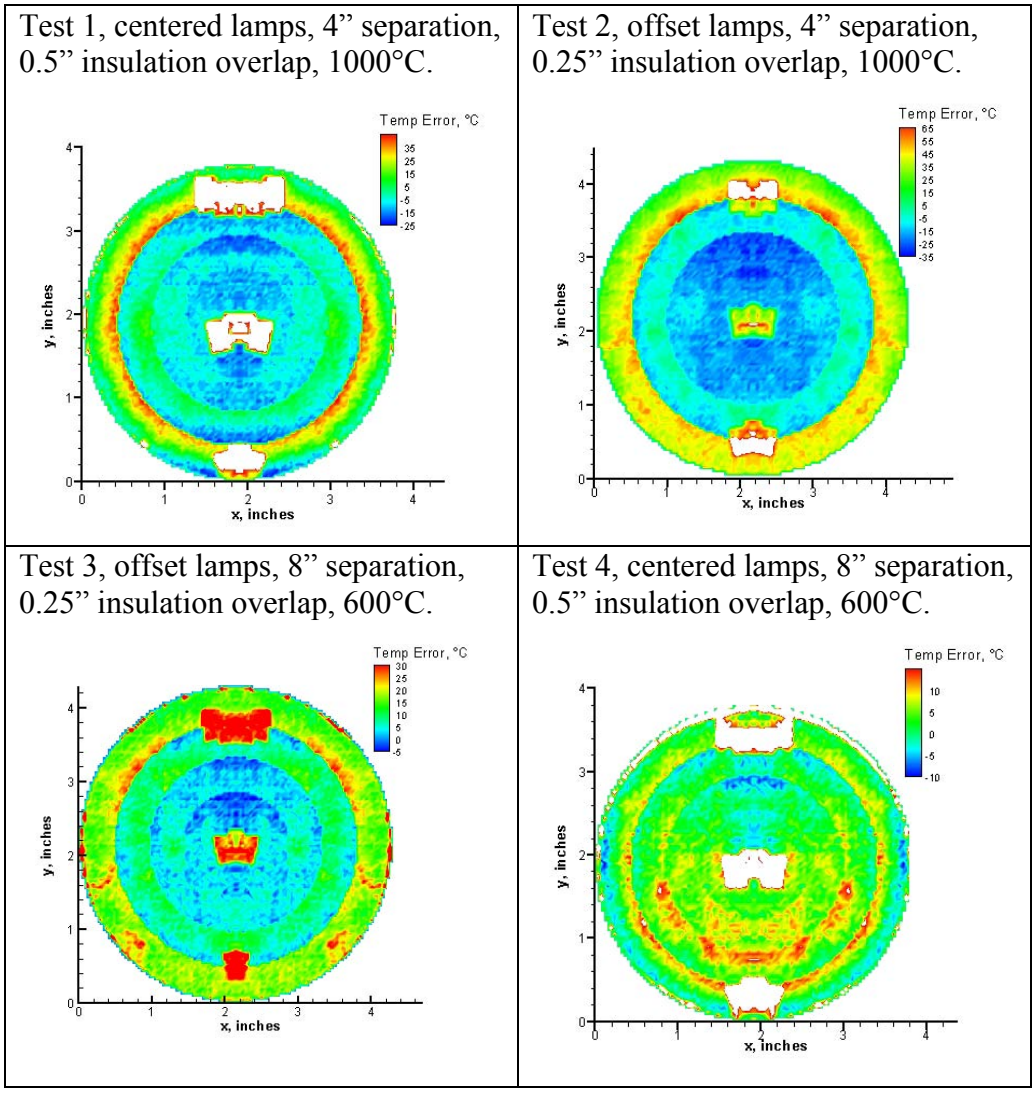

Figure 23: Tests 1 – 4 error plots. (left to right, top to bottom)

For the rectangular shroud (Figure 24) edges of SPLASH area elements are also generally visible in the error maps. The presence of the TC leads in the images is apparent. The Test 6 result demonstrates the greatest lack of symmetry in the error which may be partially due to lack of uniformity in the shroud emissivity (see discussion in 3.5.2).

For both Figure 23 and Figure 24 most of the perimeter of the shroud indicates that model temperature prediction is below the experimental observation. However, blotches of the red end of the color spectrum do show on the perimeters but these regions are too small to be credible (the very local temperature gradients would be immense) and are probably due to some interaction of radiation leaving the shroud with the materials forming the corner adjacent to the shroud.

Test 5, centered lamps, 4” separation, 0.25” insulation overlap, 600°C.

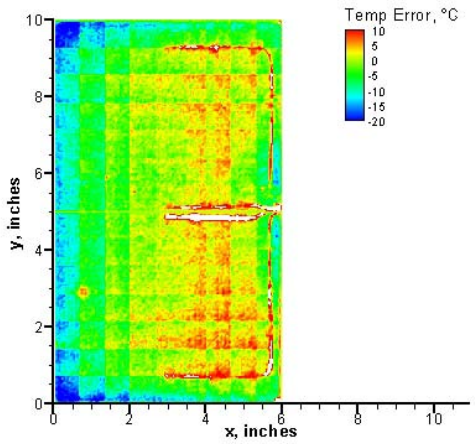

Test 6, offset lamps, 4” separation, 0.5” insulation overlap, 600°C.

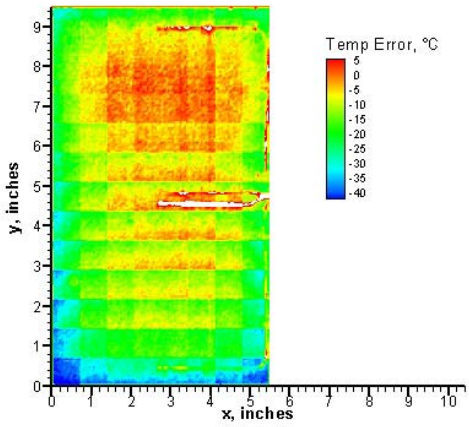

Test 7, offset lamps, 8” separation, 0.5” insulation overlap, 1000°C.

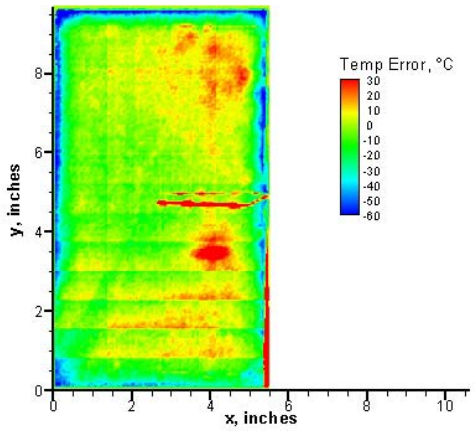

Test 8, centered lamps, 8” separation, 0.25” insulation overlap, 1000°C.

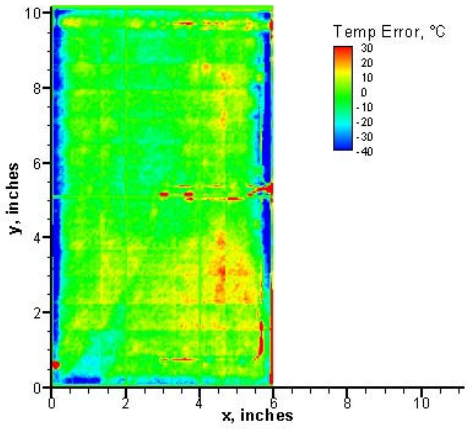

Figure 24: Error plots for tests 5 – 8 (left to right, top to bottom).

3.5 Discussion of Results

Now that we know what variables were significant contributors to temperature error, we turn our attention to understanding why these variables are significant. Four major phenomena contributing to the overall error were:

1. Model approximations

2. Emissivity variation
3. Thermocouple interference
4. Discretization of the shroud

3.5.1 Model Approximations

The radiation model has several key approximations as stated above. Two approximations that may explain the results are:

Diffuse gray panel surface
Strip heaters instead of lamps

Diffuse gray surfaces absorb and reflect radiation diffusely, i.e. equally in all directions. Polished aluminum has an emissivity as low as .06 and reflects well in the infrared spectrum. The normal spectral reflectivity of polished aluminum is shown in Figure 25. This data (Ref. [7]) is only for room temperature aluminum and does not show reflectivity data at other angles of incidence and reflection. However, the high reflectivity implies that a specular model would be more likely to capture the actual energy exchange. Fully specular models such as Monte Carlo are computationally expensive, however, and thus would not be conducive with a tool intended for use on site by a technician, an advantage that SPLASH offers.

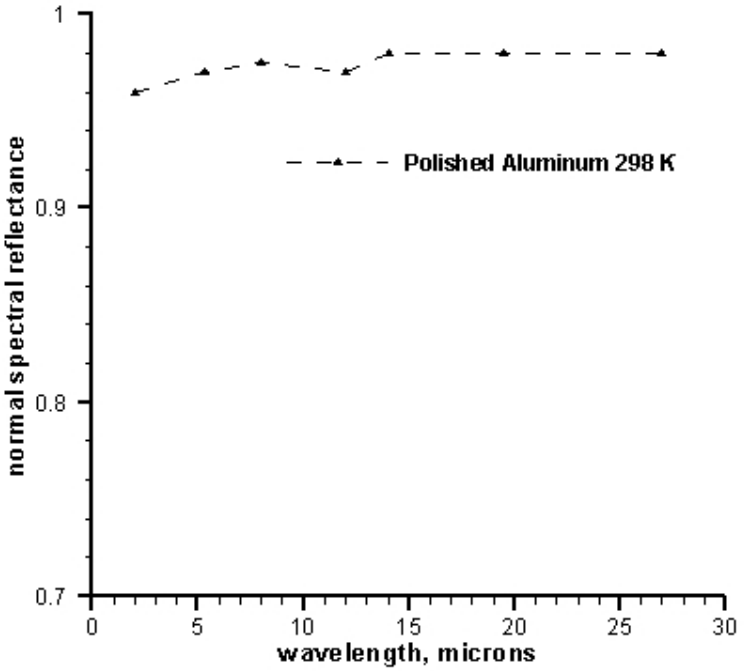

Figure 25: Reflectivity data for polished aluminum.

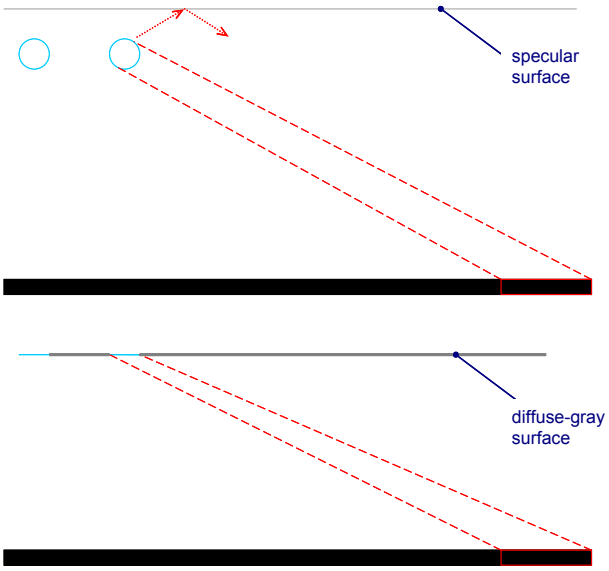

Figure 26: Comparison of actual lamp panel and modeled lamp panel energy exchange with the shroud.

The view factor for a strip heater to the shroud is significantly different from the view factor from a cylindrical lamp to the shroud. The difference is more acute at large angles. This is illustrated in Figure 26. Figure 27 shows the difference in energy exchange for a cylindrical lamp with reflection from the panel is illustrated versus energy exchange with a strip heater with no reflection from the panel. A configuration calculation was made using a two dimensional model to analyze the change in energy exchange for the two different scenarios. The configuration calculations were made using Hottel's string method (See Ref. [8]) for the strip element and configuration factor 27 from Thermal Radiation Heat Transfer for the cylinder. The abscissa starts with the lamp or strip directly over the shroud element. The distance represents the offset from this point in inches. Notice how the configuration factor for a strip falls off faster than that of a cylinder. The diameter of the cylinder and the width of the strip heater were equal at 0.2 inches. The shroud element width was 0.25 inches. The separation between the lamps or strips and the shroud was 4 and 8 inches respectively.

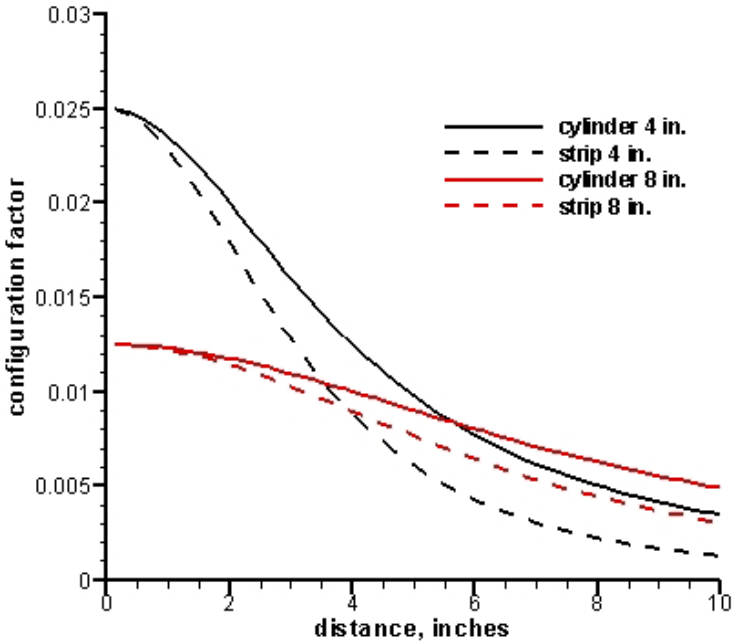

Figure 27: Configuration factor comparison for a cylinder and a strip at two separations.

3.5.2 Emissivity Variation

Figure 28 and Figure 29 show that the paint baked off of the rectangular shroud at higher temperatures resulting in a lower emissivity. In Figure 28, the picture at left was taken over two hours before the picture at right and only the corners have paint removed. After running the final tests at 1000°C, it is evident that most of the Pyromark paint is gone (right).

In Figure 29 notice that the paint has been removed first (left) from the side of the shroud with the most lamps (offset case). Higher temperatures on this side of the shroud baked off the paint. After several more tests above 1000°C (right), all of the paint has been removed.

What is not clear is why a similar reduction in emissivity did not occur for the circular shroud at the same temperatures. One explanation is that the painting, drying and curing processes were slightly different for the two shrouds.

Figure 28: Paint removal from top surface of rectangular shroud.

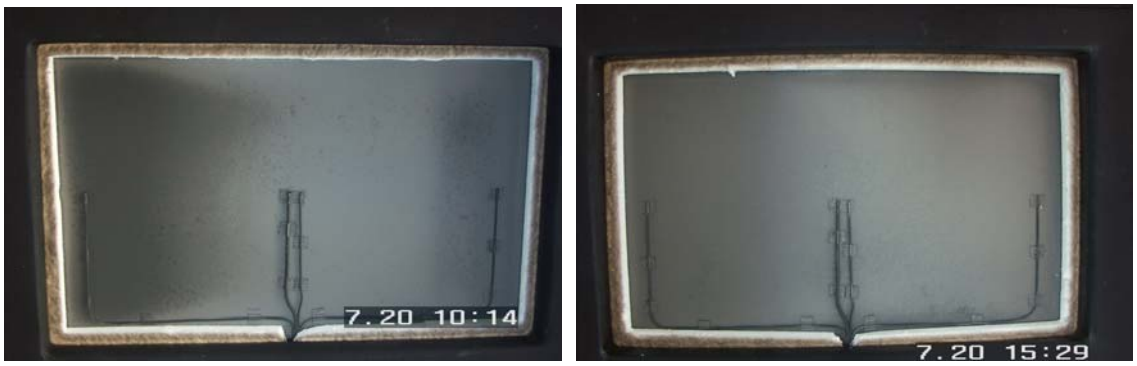

Figure 29: Paint removal from bottom surface of rectangular shroud.

Uncertainties in the emissivity were estimated by comparing the IR camera calculated temperatures with the TC readings at the three bottom thermocouple locations. Table 6 shows the relative error for each location. Notice the large discrepancies in tests 7a and 7b. This reveals the removal of Pyromark from the all but one thermocouple location. The increase in temperature error is shown in Figure 24.

3.5.3 Thermocouple Interference

The influence on the overall error due to shroud type may have been largely due to thermocouple interference in the IR image. This can be seen best in Figure 23. The thermocouples were sources of error as they were at much lower temperatures than the surrounding shroud. This effect was much greater in the circular shroud test due to the smaller size of this shroud and the larger number of thermocouples instrumented on the shroud. To ameliorate this contribution to the error, symmetry was enforced. Since along the length of the panel, both sides of the shroud should experience the same energy exchange, when the IR image was mapped, the side of the shroud with the thermocouple wires was replaced by a mirror image of the other side of the shroud. This enabled a more accurate calculation of the overall temperature error for the shroud. Although this error was reduced in this way, the larger percentage of thermocouple interference in the circular shrouds indicates that the shroud type may not have a significant influence on the overall error of SPLASH.

Table 6: Relative error between 0.063" thermocouple readings and IR camera readings after emissivity correction.

Test	(IR - B1)/IR	(IR - B2)/IR	(IR - B3)/IR
1a	0.032	0.040	0.031
1b	0.049	0.057	0.036
2a	0.040	0.058	0.045
2b	0.058	0.067	0.049
3a	0.039	0.046	0.043
3b	0.034	0.042	0.029
4a	0.041	0.033	0.026
4b	0.039	0.044	0.036
	(IR - B1)/IR	(IR - B3)/IR	(IR - B4)/IR
5a	0.019	0.022	0.006
5b	0.018	0.022	0.005
6a	0.021	0.028	0.009
6b	0.023	0.026	0.016
7a	0.007	0.045	-0.017
7b	0.009	0.048	-0.019
8a	0.011	0.052	0.002
8b	0.008	0.053	0.002

4 Conclusions

The experimental comparison demonstrated clearly that SPLASH is largely successful in predicting steady temperature distributions in lamp and shroud systems. Although clear concessions are made to keep the model tractable (for example, lamps are strips) the maximum temperature errors found were less than ±60°C. Typical errors encountered over the shroud were ±25°C. The largest errors were seen along the edge of the shroud. This was probably partly due to the mis-match in modeled and experimental "insulation overlap." Observations and probable explanations are summarized in

Table 7: Summary of observations and possible explanations.

Observation	Source	Explanation(s)
Sensitive to lamp offset—offset lamps generally yielding higher RMS error.	Figure 20	Heater geometry is simplified to strips (see Figure 26 and Figure 27) and diffuse surface approximation might be less good for high incidence angles.
Sensitive to shroud geometry—rectangular shroud yielded lower error.	Figure 20	Circular shroud was smaller and more heavily impacted by TC leads. Perimeter effects were greater on smaller shroud.
Sensitive to lamp height—greater separation usually yielding lower error.	Figure 20	Ignored geometry detail (see Figure 26 and Figure 27) and lower incidence angles for greater lamp separation.
Not sensitive to insulation overlap.	Figure 20	More sensitivity may have been seen if a finer grid had been used in the SPLASH modeling to resolve gradients near shroud edges. Shroud area coincident with insulation overlap not in RMS measure of error.
Interaction between lamp geometry and lamp separation.	Figure 20	Details of lamp geometry fade with distance.
Interaction between lamp geometry and temperature.	Figure 20	May have been contributed to by Pyromark bake-off.

Presently, no interaction with a target beneath the shroud is modeled in SPLASH and clearly some test conditions will be importantly influenced by such interaction. Nonetheless, SPLASH is a robust and useful model which can be used to investigate proposed lamp, panel, and shroud experimental configurations. The ability to get in the neighborhood of the desired design before running an actual test should save time and money for future test setup development.

The addition of a simple target to interact with the current single panel SPLASH model may be a logical extension of this work. It would be best to limit this target a simple shape or two easily defined parametrically like the rest of the features in the current SPLASH model. Addition of a capability to interact with a target probably also implies increased interest in transient response. Consequently, this effort should be considered in concert with improving the currently unsatisfactory representation of the heater control system.

5 References

1. R.I. Controls, Drawing number D49083, *Modular Heater Assembly*, May, 1986.
2. Larsen, M.E., SPLASH User's Manual, SAND Report in preparation, May, 2005.
3. National Instruments, *BridgeView and LabView PID Control Toolkit for G Reference Manual*, Part Number 320563B-01, January, 1998.
4. Nakos, J. T., J. M. Suo-Anttila, W. Gill, "Shroud Boundary Condition Characterization Experiments at the Radiant Heat Facility" SAND2004-5080, October, 2004.
5. Nakos, J. T., "Uncertainty Analysis of Thermocouple Measurements Used in Normal and Abnormal Environment Experiments at Sandia's Radiant Heat Facility and Lurance Canyon Burn Site," SAND2004-1023, Sandia National Laboratories, April, 2004.
6. *Minitab Reference Manual Release 9* Sowers Printing Company, Lebanon, PA, USA .
7. Touloukian, Y. S., DeWitt, D. P. Thermal Radiative Properties Metallic Elements and Alloys. Volume 7 in series: Thermophysical properties of matter. IFI/Plenum. New York. Pg 20-34 & 1104-1110.
8. Siegel, Robert, Howell, John R. "Thermal Radiation Heat Transfer" 4th ed. 2002. Taylor & Francis, New York.
9. Howell, John R., A Catalog of Radiation Heat Transfer Configuration Factors, http://www.me.utexas.edu/~howell/.

Appendix A—View Factor Calculation

5.1 Finite Rectangles

5.1.1 Finite Rectangle to Finite Rectangle

The most commonly required view factor in SPLASH calculations is that between parallel, finite rectangles as shown in Figure 30. Equation (20) [9] was used for such geometries.

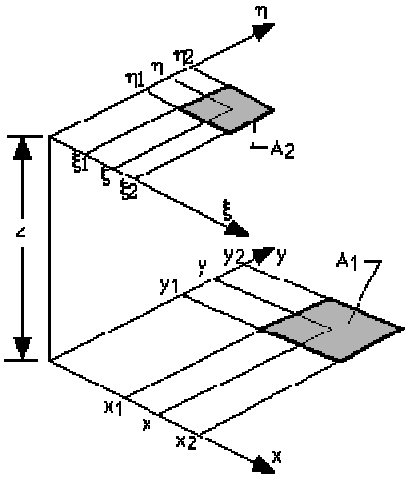

Figure 30: Coordinates/schematic for view factor calculation between finite rectangles.

$$F_{1-2} = \frac{1}{(x_2 - x_1)(y_2 - y_1)} \sum_{l=1}^{2}\sum_{k=1}^{2}\sum_{j=1}^{2}\sum_{i=1}^{2} (-1)^{(i+j+k+l)} G(x_i, y_j, \eta_k, \xi_l)$$

$$G = \frac{1}{2\pi}\left(\begin{array}{l} (y-\eta)\left[(x-\xi)^2 + z^2\right]^{1/2} \tan^{-1}\left\{ \dfrac{y-\eta}{\left[(x-\xi)^2 + z^2\right]^{1/2}} \right\} \\ +(x-\xi)\left[(y-\eta)^2 + z^2\right]^{1/2} \tan^{-1}\left\{ \dfrac{x-\xi}{\left[(y-\eta)^2 + z^2\right]^{1/2}} \right\} \\ -\dfrac{z^2}{2} \ln\left[(x-\xi)^2 + (y-\eta)^2 + z^2\right] \end{array} \right) \quad (20)$$

5.1.2 Area Element to Finite Rectangle

In systems using circular shrouds it was necessary to perform numerical integration over the finite areas formed by radials and arcs. Such areas never "see" each other so it was sufficient to have an expression for the view from a differential area to a parallel finite rectangle. Figure 31 shows the geometry corresponding to Equation (21) which provides the associated view factor when the differential area is located on a normal from one corner of the finite rectangle.

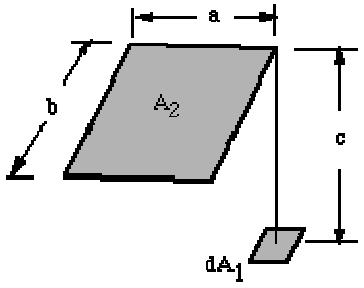

Figure 31: Coordinates/schematic for view factor calculation between finite rectangle and an area element.

$$F_{d1-2} = \frac{1}{2\pi}\left\{\begin{array}{l} \dfrac{A}{\left(1+A^2\right)^{1/2}}\tan^{-1}\left[\dfrac{B}{\left(1+A^2\right)^{1/2}}\right] \\ +\dfrac{B}{\left(1+B^2\right)^{1/2}}\tan^{-1}\left[\dfrac{A}{\left(1+B^2\right)^{1/2}}\right] \end{array}\right\} \tag{21}$$

Where $A = a/c$ and $B = b/c$.

5.1.3 View Factor Algebra

Equation (21) was not sufficiently general and view factor algebra was required to provide the more general case of dA_1 not lying on a normal at one corner of the rectangle of interest. For example, consider the geometry of Figure 32 and the case in which the view of dA to A_1 is required.

Then

$$dF_{dA,A_1} = dF_{dA,A_1+A_2+A_3+A_4} - dF_{dA,A_3+A_4} - dF_{dA,A_2+A_4} + dF_{dA,A_4} \tag{22}$$

Similar expressions are apparent for other cases, such as when dA lies within the extent of one of the length or width of the finite rectangle.

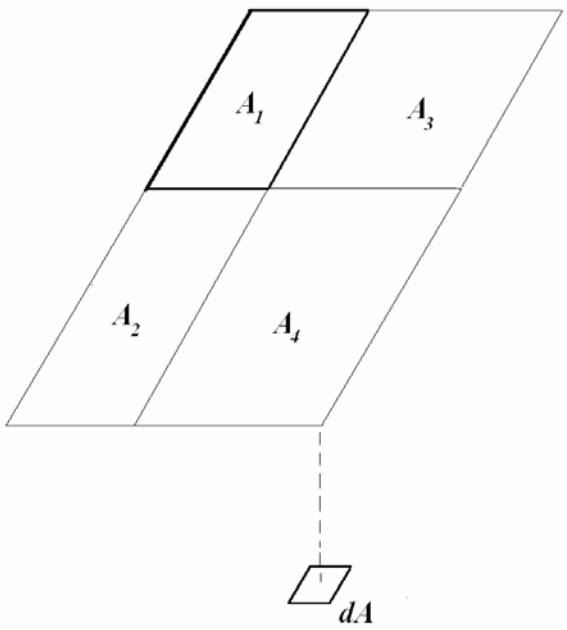

Figure 32: Geometry illustrating view factor algebra.

5.2 Non-rectangular Finite Areas

5.2.1 Numerically Integrating Over Round Shroud Sectors

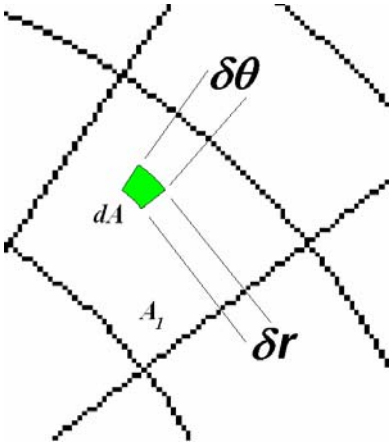

Figure 33: Sector geometry for an element on a circular shroud.

Figure 33 shows a typical element of a circular shroud. A simple numerical summation of sub-areas is used to produce the required integration. So for some finite area, A_2, the view factor from A_1 to A_2 is:

$$F_{12} \cong \frac{1}{A_1} \sum\sum dA \; dF_{dA,A_2}\left(r_i, \theta_j\right) \tag{23}$$

Where the sums represent steps in the r and θ directions.

5.2.2 Approximating Rectangles Eclipsed by Arcs

Figure 34 shows a complication that results when a circular shroud lies atop of the rectangular grid describing the underlying insulation. SPLASH lays out the grid describing the insulation first. In the left part of the figure the rectangular elements that are intersected by the circular shroud are shaded. As the user independently chooses the shroud and insulation properties rectangular elements eclipsed by the round shroud are produced. These shapes are treated approximately in the radiation enclosure problem. The right part of Figure 34 has heavier black lines that represent the rectangles substituted for the misshapen elements beneath. These "surrogate" rectangles are used for the purposes of calculating view factors. The surrogate rectangles have the same centroid location, area, and 2nd area moment about the x-axis as the polygons they replace.

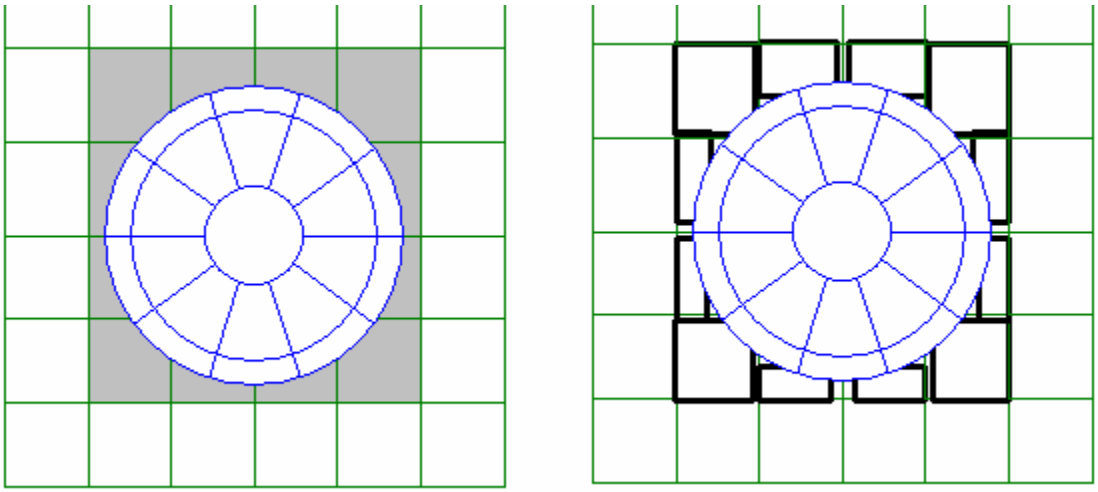

Figure 34: Geometry of circular shroud atop rectangular insulation (left) and "equivalent" rectangles.

5.3 View Factor Reciprocity and Conservation

At the lamp panel plane all the enclosure areas are rectangular. The reciprocity relation $\left(A_i F_{ij} = A_j F_{ji}\right)$ is used to find view factors from those surfaces back to any irregular area in the plane of the shroud or insulation.

After the use of the foregoing expressions, integration, reciprocity, and assertion that same-plane areas have zero view to each other the only unspecified view factors are those describing views to the environment. Those are all calculated using conservation, that is:

$$F_{iN} = 1 - \sum_{j=\text{all but } N} F_{ij} \qquad (24)$$

Finally, the view factors from the environment to the areas defined in the system are evaluated using reciprocity.

Distribution

1	MS 0824	9110	Wahid Hermina
1	MS 0836	9116	Amanda Barra
1	MS 0836	9116	Barry Boughton
1	MS 0836	9116	Aaron Brundage
1	MS 0836	9116	Dean Dobranich
1	MS 0836	9116	Bill Erickson
1	MS 0836	9116	Nick Francis
1	MS 0836	9116	Gene Hertel
1	MS 0836	9116	Roy Hogan
1	MS 0836	9117	Richard Griffith
10	MS 0836	9117	Marvin Larsen
1	MS 0824	9130	T.Y. Chu
1	MS 1135	9132	Pat Drozda
1	MS 0836	9132	Walt Gill
1	MS 0821	9132	Lou Gritzo
1	MS 1135	9132	Chuck Hanks
1	MS 1135	9132	Dann Jernigan
1	MS 1135	9132	Jim Nakos
1	MS 0836	9132	Cecily Romero
1	MS 1135	9132	Jill Suo-Anttila
1	MS 1135	9132	Richard Streit
1	MS 0828	9133	Kevin Dowding
1	MS 0828	9133	Martin Sherman
1	MS 9018	8945-1	Central Technical Files
2	MS 0899	9616	Technical Library

External: John R. Howell
The University of Texas at Austin
Department of Mechanical Engineering
1 University Station, C2200
Austin, TX 78712-0292